TECHNISCHE UNIVERSITÄT WIEN
Vienna University of Technology

VIENNA UNIVERSITY OF TECHNOLOGY

INSTITUTE OF ENERGY SYSTEMS AND THERMODYNAMICS

MASTER THESIS

Efficiency scale-up of reactor coolant pumps

Carried out for the purpose of obtaining the degree of Master of Science (MSc or Dipl.-Ing) of Mechanical Engineering

under the supervision of

Ass.Prof. Dipl.-Ing. Dr.techn. Klaus Käfer
and
Univ.Prof. Dipl.-Ing. Dr.-Ing. Christian Bauer

Author: **Mattia Tasinato**

Student ID: **1227014**

Study Code: **E 066 445**

Vienna, July, 2018 .....

Abstract

The scale-up procedure for hydraulic machinery is currently regulated by two international standards: IEC 60193 and IEC 62097. The accepted standards are two since the newer one (IEC 62097) isn't applicable to all types of machines, due to the lack of sufficient studies. Reactor coolant pumps (RCPs) are part of the machines not covered by the new standard, and therefore still have to be scaled-up with the less accurate method, presented in the older norm.

This work aims to determine the needed scale-up factors to apply the new standard IEC 62097 to axial-flow RCPs, through the study of two such pumps. The methods used vary for each component since different approaches are needed to estimate in an accurate, yet non-overcomplicated way the friction losses (scalable losses), according to the geometry and flow dynamics of the component. Hence, the friction losses of runner blades and guide vanes are calculated with the friction loss factor of a flat plate, while for the casing sections of runner blades and guide vanes the loss coefficient formula of Nichtawitz is used. The friction losses of the cylindrical casing, due to the complex flow dynamics, are determined by performing a CFD-analysis. Lastly, the shroud ring losses are obtained through the loss coefficient for two concentric rotating cylinders. It is to note, that the shroud ring losses are relevant only for one of the two studied pumps, as solely the Type 1400 RCP is provided with a shroud ring. The results are then combined into linear functions which describe the scale-up factors according to the specific speed of the machine. Finally, the scale-up formulas presented in the standard IEC 620197, are adapted according to the new component subdivision of axial RCPs.

By performing scale-up calculations with the new method, an efficiency increase from model to prototype of roughly 2,1% was determined. This result differs from the efficiency increase of roughly 5% calculated with the standard IEC 60193 and therefore confirms the fact that the older norm overestimates the efficiency increase. Through the comparison of scale-up calculations with different wall roughnesses, it was also possible to investigate the wall roughness effects on the scale-up, which showed that rougher prototype wall roughnesses decrease the efficiency increase.

Kurzfassung

Das Verfahren zur Leistungsaufwertung hydraulischer Maschinen wird derzeit durch die internationalen Normen IEC 60193 und IEC 62097 geregelt. Die anerkannten Normen sind zwei, da die neuere (IEC 62097) nicht an allen Maschinentypen anwendbar ist. Reaktorkühlpumpen (RCPs) sind Teil der Maschinen, die nicht von der neuen Norm abgedeckt werden und müssen deshalb weiterhin mit der ungenaueren Methode der älteren Norm aufgewertet werden.

Das Ziel dieser Arbeit ist es, die zur Anwendung der neuen IEC 62097 Norm notwendigen Aufwertungsfaktoren für axiale RCPs durch die Studie zwei solcher Pumpen zu bestimmen. Die dafür eingesetzten Methoden variieren je nach Geometrie und Strömungsdynamik der Komponenten, da unterschiedliche Ansätze zur genauen und dennoch nicht überkomplizierten Abschätzung der Reibungsverluste (aufwertbare Verluste) notwendig sind. Die Reibungsverluste der Lauf- und Leitschaufeln werden daher mit dem Reibungsverlustfaktor einer ebenen Platte berechnet, während für die ringförmigen Gehäuseteile vom Leit- und Laufrad die Verlustkoeffizienten-Formel von Nichtawitz verwendet wird. Die Reibungsverluste des zylindrischen Gehäuses werden aufgrund der komplexen Strömungsdynamik durch eine CFD-Analyse ermittelt und die Deckbandverluste des Laufrades durch den Verlustkoeffizient für zwei konzentrisch rotierende Zylinder. Aus den Ergebnissen werden dann linearen Funktionen extrapoliert, die die Aufwertungsfaktoren gemäß der spezifischen Drehzahl der Maschine beschreiben.

Durch Anwendung der neuen Aufwertungsmethode für axiale RCPs wurde eine Wirkungsgradsteigerung von Modell zu Prototyp von 2,1% ermittelt. Dieses Ergebnis unterscheidet sich wesentlich von der 5% Wirkungsgradsteigerung, die mit der Norm IEC 60193 erhalten wird und bestätigt damit die Tatsache, dass die ältere Norm die Wirkungsgradaufwertung überschätzt. Mittels Vergleiche von Wirkungsgradaufwertungen mit unterschiedlichen Wandrauhigkeiten konnten auch die Wandrauhigkeitseinflüsse im Aufwertungsprozess untersucht werden und es ergab sich, dass gröbere Prototyp-Wandrauhigkeiten die Wirkungsgradsteigerung verringern.

List of subscripts

Subscript	Definition	Subscript	Definition
amb	Ambient conditions	u	Velocity or peripheral
d	Dimension	W	Water
E	Specific energy	**Components subscripts**	
f	Friction	CO	Component
h	Hydraulic	CY	Cylindrical casing
k	Kinetic	DT	Draft tube
L	Loss	GV	Guide vanes
m	Meridian	GVC	Annular guide vane channel
M	Model	GVS	Guide vane section
opt	Optimum point	RB	Runner blades
P	Prototype	RUC	Annular runner channel
PS	Pressure side	RU	Runner
Q	Volumetric	SP	Spiral case
ref	Reference	SR	Shroud ring
SS	Suction side	SV	Stay vane
T	Torque or disc/ shroud ring friction		

List of symbols

Symbol	Unit	Definition
A_{CO}	$[m^2]$	Sectional area of the flow of the component
A_1	$[m^2]$	Area of the pressure side measuring section
A_2	$[m^2]$	Area of the suction side measuring section
B_{CO}	[m]	Component width
b	[m]	Average clearance between rotating cylinders
c	$[\frac{m}{s}]$	Absolute flow velocity in the runner
c_u	$[\frac{m}{s}]$	Absolute peripheral flow velocity in the runner
c_m	$[\frac{m}{s}]$	Absolute meridian flow velocity in the runner
C	[-]	Discharge coefficient, obtained from the calibration as a function of Reynolds number
C_f	[-]	Friction coefficient for flat plates
C_T	[-]	Friction coefficient for concentric rotating cylinders
D	[m]	Reference diameter of the hydraulic machine
d_h	[m]	Hydraulic diameter
d_V	[m]	Nominal diameter of Venturi tube
E_h	$[\frac{m^2}{s^2}]$	Specific hydraulic energy

E_{LF}	$[\frac{m^2}{s^2}]$	Friction loss of specific hydraulic energy
F_f	[N]	Friction force
F_L	[N]	Reaction force
g	$[\frac{m}{s^2}]$	Acceleration due to gravity at the testing location
H	[m]	Net head
L_{CO}	[m]	Component length
n	$[\frac{1}{s}]$	Rotational shaft speed
N_{QE}	[-]	Specific speed
$NPSE$	$[\frac{m^2}{s^2}]$	Net positive suction energy
p_{amb}	[Pa]	Ambient pressure
p_Q	[Pa]	Pressure difference at Venturi tube
p_{12}	[Pa]	Static pressure difference between high and low pressure measuring section
p_2	[Pa]	Absolute static pressure at the suction side
p_{VA}	[Pa]	Vapor pressure
P_h	[W]	Hydraulic power
P_m	[W]	Mechanical power
P_L	[W]	Mechanical power loss
Q	$[\frac{m^3}{s}]$	Discharge

R_L	[m]	Lever arm length
Ra	[m]	Wall roughness
Re	[-]	Reynolds number
$R\omega$	[-]	Rotational Reynolds number
S_{CO}	$[m^2]$	Wall surface area of the component
t_W	[°C]	Water temperature
T	$[N \cdot m]$	Hydraulic torque
u	$[\frac{m}{s}]$	Peripheral velocity
v_{CO}	$[\frac{m}{s}]$	Mean velocity of the component
w	$[\frac{m}{s}]$	Relative flow velocity in the runner
V_{ref}	[-]	Reference loss distribution coefficient
Z_{CO}	[-]	Number of blades/vanes of the component
β	[°]	Relative velocity angle
δ	[-]	Ratio of scalable losses
δ_{ns}	[-]	Ratio of non-scalable losses
$\delta_{E,CO,ref}$	[-]	Reference scalable hydraulic energy loss for each component
Δ	[-]	Ratio of efficiency step-up against model efficiency
$d_{E,CO,ref}$	[-]	Scalable hydraulic energy loss index for each component

ζ_1	[-]	Pressure side loss coefficient
ζ_2	[-]	Suction side loss coefficient
η_h	[-]	Hydraulic efficiency
η_E	[-]	Specific hydraulic energy efficiency
η_Q	[-]	Volumetric efficiency
η_T	[-]	Power efficiency (disc friction efficiency)
$\Delta\eta_{M->P}$	[-]	Efficiency difference between model and prototype
$\kappa_{d,CO}$	[-]	Dimension factor for each component
$\kappa_{u,CO}$	[-]	Flow velocity factor for each component
κ_T	[-]	Dimension factor for disc friction loss
λ	[-]	Friction loss coefficient for a channel
ν_W	$[\frac{m^2}{s}]$	Water kinematic viscosity
ρ_W	$[\frac{kg}{m^3}]$	Water density at testing conditions
σ	[-]	Thoma number
ω	$[\frac{1}{s}]$	Rotational speed

Contents

1 Introduction

Reactor coolant pumps (RCP) are essential components of nuclear power plants. They keep the reactor core at the right temperature to ensure its safe and controlled operation and transfer the absorbed heat to steam generators, which produce the output energy of the plant. Due to the high temperatures of up to 300°C and pressures of 160 bar, it is crucial to have RCPs with a reliable and efficient design, whose state can be monitored easily during operation [1]. Before the production of a full-size prototype begins, scaled models are produced and tested to ensure and assess these critical characteristics. The prototype performance data is then obtained, by transposing the data of the tested model to the full-size machine.

The scale-up procedure for hydraulic machinery is currently regulated by two international standards: IEC 60193 and IEC 62097. In the older standard IEC 60193, a constant scale-up factor V_{ref} in used, indicating the percentage of scalable losses in each type of machine. This scale-up method is very simple and easy to apply but contains multiple inaccuracies, which benefit machines with lower design quality, and it overestimates the efficiency increase. For these reasons, in 2009 the standard IEC 62097 was introduced. The new standard improved the scale-up procedure by considering each component individually, including the wall roughness, and utilizing scale-up factors which vary according to the specific speed. The downside of this standard is that, so far, it can't be applied to all types of hydraulic machines, including reactor coolant pumps. The reason being that the needed flow velocity factors, dimension factors, and scalable hydraulic energy loss indexes, haven't been derived and studied for all types of hydraulic machines.

To obtain these factors for axial working RCPs a loss analysis of each major component is necessary. Losses have to be categorized into scalable and non-scalable losses, whereas friction and leakage losses are considered as scalable and kinetic losses as non-scalable losses [4]. They can be calculated with different approaches, depending on the geometry and type of flow of the investigated part. For channels, flat plates, concentric rotating cylinders, and disks, existing formulas for friction coefficients give a good estimate of the losses, while for components with more

complex geometries and flow dynamics, like cylindrical casings, a CFD flow analysis is more suitable to obtain accurate results. Once multiple machines of the same type have been studied, the obtained results can be combined into linear functions which define the scale-up coefficients according to the specific speed of the machine.

1.1 Problem outline and solution approach

The objective of this work is to determine the needed scale-up coefficients for axial working RCPs so that the performance scale-up can be computed with the new international standard IEC 62097, instead of the older and less accurate standard IEC 60193. Measured data of two RCP models, provided by the company *ANDRITZ AG*, is used to perform the study. To obtain an applicable version of the standard IEC 62097 for axial working RCPs, the following steps are required:

- Conducting a loss analysis of the main components of the two pumps
  - Dividing the reactor coolant pumps into main components
  - Finding suitable friction factor formulas for the components with similar flow dynamic and geometry to commonly studied flows
  - Performing a CFD analysis with the commercial software *ANSYS Fluent* of the cylindrical casings to determine the scalable losses of these more complex components
- Calculating the scale-up coefficients for the two pumps at optimum efficiency point and combining the results into linear functions depending upon the specific speed of the machines
- Adapting the scale-up formulas in the IEC 62097 standard to the utilized formulas for the friction factors

With the obtained results, scale-up calculations should be made to compare the efficiency increase between the two standards and assess their accuracy.

2 Reactor coolant pumps (RCPs)

The studied reactor coolant pumps are employed in the primary coolant loop of pressurized-water reactors. These type of reactors are light water reactors since they utilize regular water as opposed to heavy water, a form of water that contains a larger amount of hydrogen isotope deuterium [14]. Figure 1 depicts a typical pressurized-water reactor with its main components. The core inside the reactor vessel generates heat that is transferred to the pressurized water in the primary coolant loop and carried to the steam generator. There, the secondary loop water is vaporized by the heat from the primary coolant loop and directed to the main turbine, which produces electricity [13].

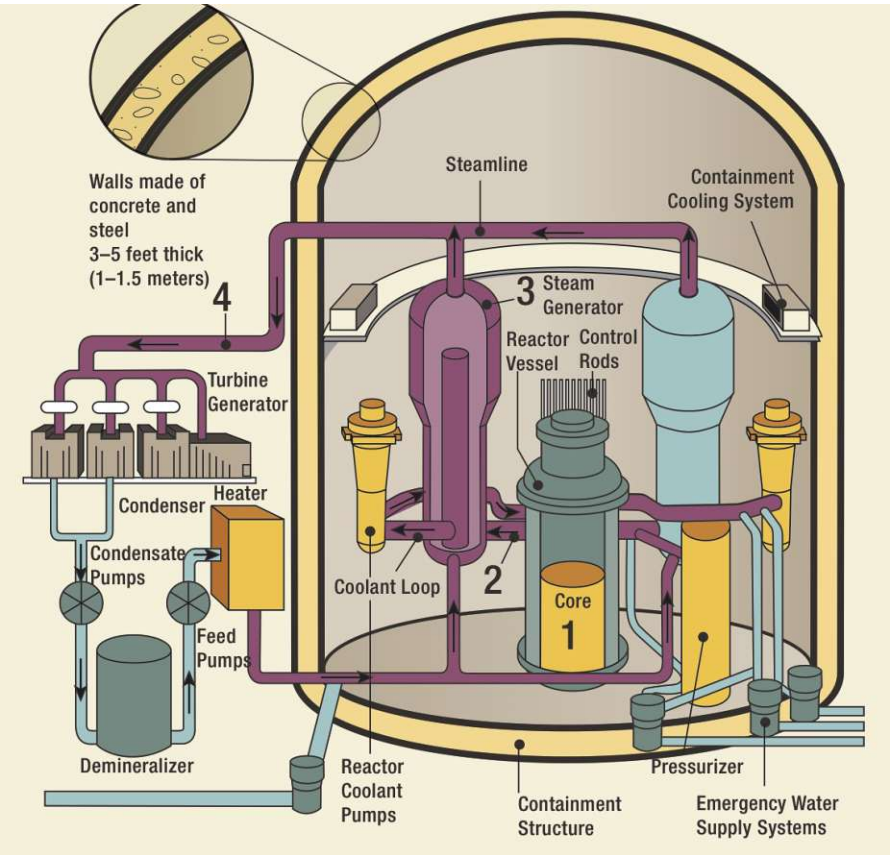

Figure 1: Pressurized water reactor [13].

The operating conditions of reactor coolant pumps are very demanding considering the pumps have to withstand operating temperatures of up to 300°C and pressures of around 16 MPa. The high pressure is necessary to avoid water evaporation in the primary loop. A large volumetric flow rate of round 6,6 m^3/s is required to ensure a sufficient and safe heat transfer inside the reactor core.

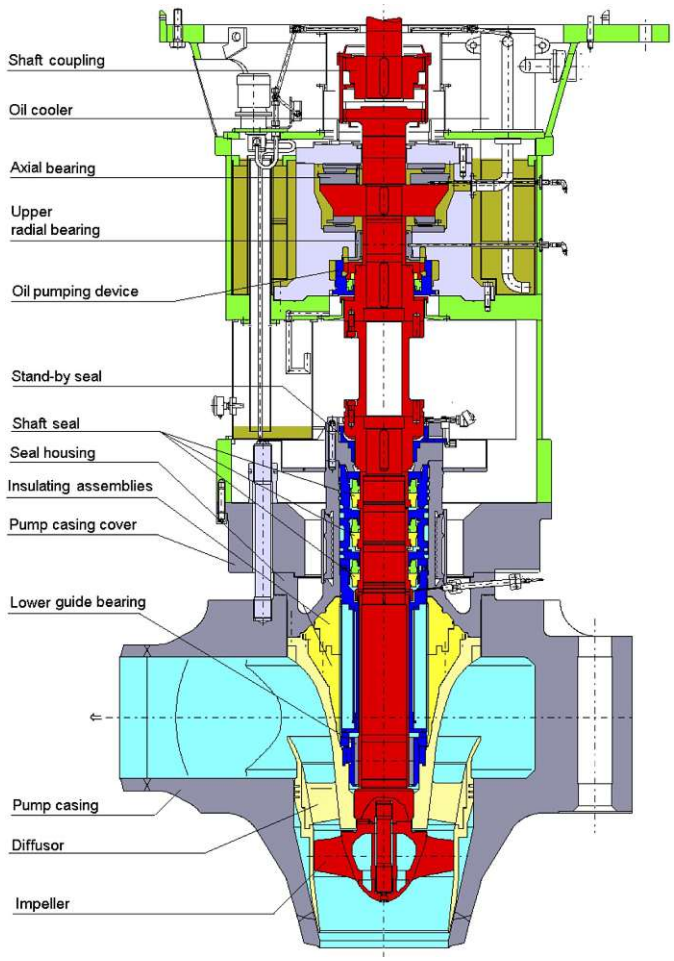

Figure 2: Reactor coolant pump components [1]

Figure 2 depicts the section plane of an axial working RCP. A tree stage mechanical face seal avoids water leakage up the shaft, which is supported by an axial bearing and centered by multiple radial bearings. The lower guide bearing and the seals

are water lubricated, while the upper slider bearings are oil lubricated [1]. During operation, the coolant passes through the impeller which accelerates the flow, while the stay vanes behind the impeller remove the generated swirl. In the cylindrical casing, the kinetic energy of the flow is converted into pressure, so that the coolant can reach the reactor core.

2.1 The investigated reactor coolant pumps

The studied reactor coolant pumps were realized by *ANDRITZ AG* and employed in different nuclear power plants. Of the two investigated pumps one is a pure axial working RCP, while the other one has a design between an axial and a mixed-flow RCP. The pure axial working RCP will be referred to as "Type 1134 RCP" and the axial/mixed-flow RCP as "Type 1400 RCP".

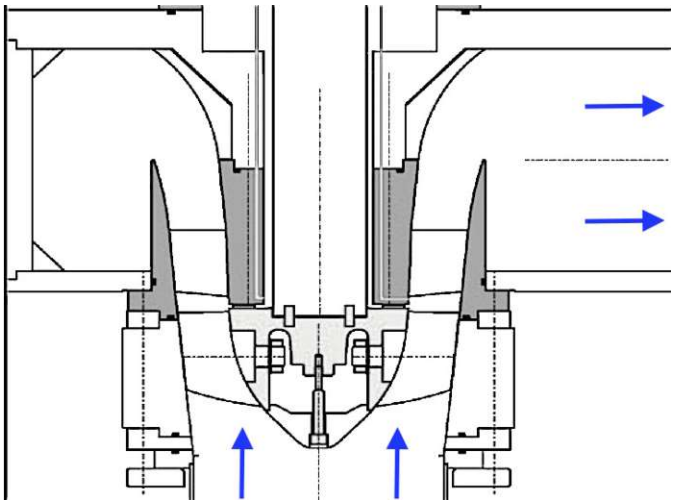

Figure 3: Type 1134 RCP [1]

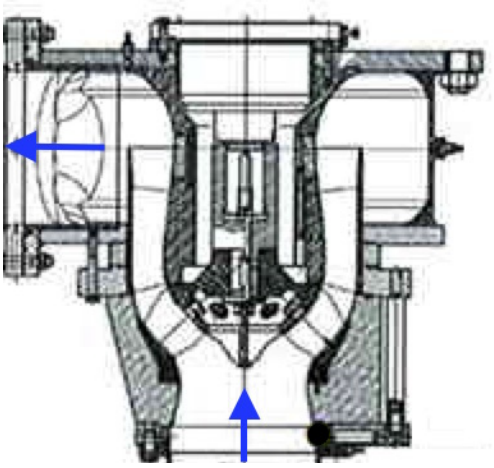

Figure 4: Type 1400 RCP [1]

Figure 3 and 4 show the two pumps and their different runner blade placement. The Type 1134 pump is a faster rotating pump, rotating at roughly 1500 rpm while the Type 1400 pump rotates slower at 1200 rpm [1]. The scaled models of the two pumps were tested at the testing facility *ASTRÖ-Laboratory* of *ANDRITZ AG* in Graz, and the acquired data was used to obtain the scale-up coefficients, as described in the following chapters.

3 Measured data

The data utilized to obtain the scale-up factors for the two pumps derive from tests conducted at the testing facility *ASTRÖ-Laboratory* of *ANDRITZ AG* in Graz. Multiple tests were carried out, including efficiency tests, cavitation tests, pressure pulsation tests, four quadrant tests, radial force and momentum tests, runaway speed tests, axial thrust tests, and trimming tests. Of the wide range of data collected, the data related to the efficiency tests are utilized.

3.1 The testing facillity

The *ASTRÖ-Laboratory* in Graz has two test rigs, the turbine test stand, and the four quadrant test stand. The model tests were conducted with the four quadrant test stand depicted in Figure 5. It consists of a closed loop designed to test axial and radial working models in a horizontal or vertical arrangement. The stand is divided into two sub-loops: the vertical section with the main booster pump and the flow meter, and the horizontal section with the second booster pump, the tested model, and the tail-water tank. In the vertical section, the flow direction is always the same, while in the horizontal section the direction can be changed by altering the flow distributor position. The pressure in the system is regulated by the pressure control unit connected to the tail-water tank, which can provide various cavitation conditions. During operation, the water is pumped with the main booster pump through the Venturi-tube inlet tank, where it passes the heat exchanger and straightener inside the tank, to the Venturi tube, where the flow-rate is measured. It then continues through the flow distributor to reach the tail-water tank and the tested model. From the model outlet, the water flows to the energy dissipator and to the flow distributor to be recirculated. The utilized water comes from the main and its temperature inside the loop is kept constant in a range of $\pm$ 2°C by a water cooler, positioned in the connection pipe between the flow distributor and the tail-water tank [1].

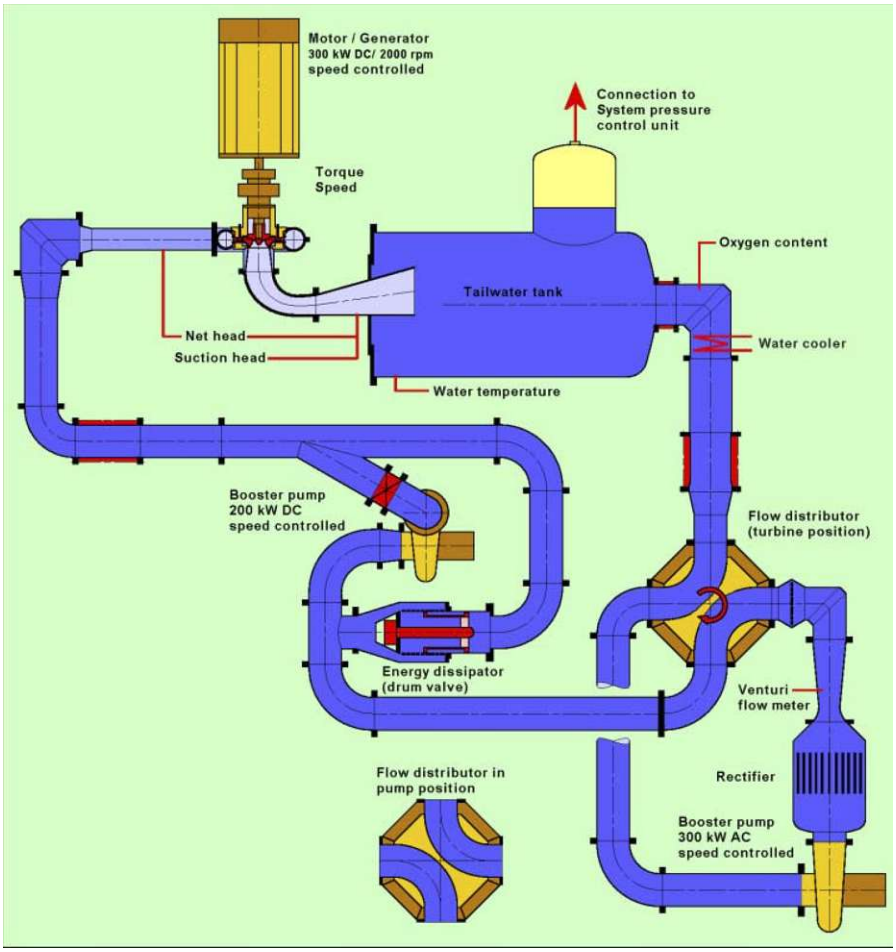

Figure 5: Four quadrant test stand at *ASTRÖ-Laboratory* of *ANDRITZ AG* in Graz [1]

3.2 Measuring instrumentation

The following sections describe the measuring instrumentation and equations to compute the discharge Q_M, net head H_M, torque T_M, rotational speed n_M, power output $P_{h,M}$, efficiency $\eta_{h,M}$, temperature t_W, net positive suction energy $NPSE_M$, and cavitation number σ for the tested model. Details about the pressure pulsation tests and axial thrust measurements are not included.

3.2.1 Discharge measurement

The discharge is measured with a Venturi tube positioned in the vertical section of the loop. The pressure difference between the Venturi tube inlet and throat is measured with a high precision rotary piston manometer. The discharge is then computed with the following relation:

$$Q_M = C \cdot \frac{d_V^2 \cdot \pi}{4} \cdot \sqrt{\frac{2 \cdot p_Q}{\rho_W}} \tag{1}$$

C is the discharge coefficient, obtained from the calibration as a function of the Reynolds number. d_V is the nominal diameter of the Venturi tube, p_Q the manometer reading, and ρ_W the density of the test water [1].

3.2.2 Net head measurement

The hydraulic specific energy is obtained through equation (2). Q_M is the discharge measured according to section 3.2.1 and p_{12} is the static pressure difference measured by a membrane transducer or a rotary piston manometer between the two measuring sections depicted in Figure 6.

$$E_M = \frac{p_{12}}{\frac{\rho_W(p_{2,M}+p_{12};t_W)+\rho_W(p_{2,M};t_W)}{2}} + \frac{(\frac{Q_M}{A_1})^2 - (\frac{Q_M}{A_2})^2}{2} + \frac{\zeta_1 \cdot (\frac{Q_M}{A_1})^2 - \zeta_2 \cdot (\frac{Q_M}{A_2})^2}{2} \tag{2}$$

The water density ρ_W used in the equation is an average of the densities at the two measuring sections. The friction loss term

$$\frac{\zeta_1 \cdot (\frac{Q_M}{A_1})^2 - \zeta_2 \cdot (\frac{Q_M}{A_2})^2}{2} \tag{3}$$

considers the losses between the measuring sections and the reference sections and has to be taken into account if the sections don't match. Once the hydraulic specific

energy E_M is determined, the net head H_M can be obtained with equation (4) [1].

$$H_M = \frac{E_M}{g_M} \tag{4}$$

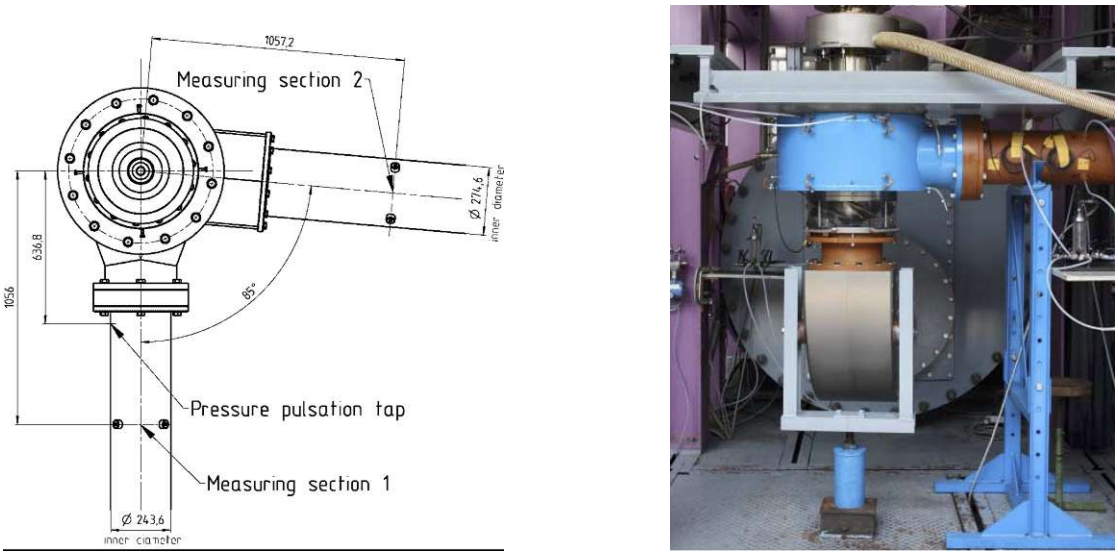

Figure 6: Position of the model measuring sections (left); arrangement of the model on the test stand (right) [1]

3.2.3 Torque measurement

The hydraulic torque of the model is defined as

$$T_M = F_{L,M} \cdot R_L. \tag{5}$$

$F_{L,M}$ is the reaction force to the model torque and is measured on an accurately calibrated lever arm with length R_L, on the oscillating part of the hydrostatically supported dynamometer. The measured torque corresponds to the torque at the coupling between model runner and shaft, since also the model runner is supported hydrostatically [1].

3.2.4 Rotational speed measurement

The rotational speed n_M is measured by an electromagnetic pickup, which transmits the pulses, received from a toothed disk mounted on the dynamometer shaft, to a quartz timer/counter. The disk generates 60 pulses per revolution, therefore, the number of rpm can be directly read on the instrument [1].

3.2.5 Power output and efficiency

With the measured torque T_M, the rotational speed n_M, the discharge Q_M, and the hydraulic specific energy $E_{h,M}$, the mechanical power $P_{m,M}$ and the hydraulic power $P_{h,M}$ can be calculated with the following equations:

$$P_{m,M} = 2 \cdot \pi \cdot n_M \cdot T_M \tag{6}$$

$$P_{h,M} = \rho_W \cdot E_M \cdot Q_M \tag{7}$$

The hydraulic model efficiency can then be calculated with [1]:

$$\eta_{h,M} = \frac{P_{h,M}}{P_{m,M}} \tag{8}$$

3.2.6 Temperature measurement

The temperature t_W is measured with a Pt-100 probe fitted into the tailwater tank and a signal conditioner connected to the test stand computer [1].

3.2.7 Net positive suction energy and cavitation number measurement

The net positive suction energy $NPSE_M$, defined in equation (9), describes the cavitational behavior of the pump [5].

$$NPSE_M = \frac{p_{2,M} - p_{VA}(t_W)}{\rho_W(p_{2M}; t_W)} + \frac{(\frac{Q_M}{A_2})^2}{2} \tag{9}$$

$$p_{2,M} = p_2 + p_{amb} \tag{10}$$

$p_{2,M}$ is the absolute pressure in the suction side measuring section and can be determined with equation (11), in which p_2 represents the suction pressure, measured by a rotary piston manometer calibrated in such a way that the reading shows the pressure against the reference point, while p_{amb} is the ambient pressure, measured by a mercury barometer [1]. The cavitation Thoma number can then be derived with the following equation:

$$\sigma = \frac{NPSE_M}{E_M} \tag{11}$$

4 Scale-up methods for hydraulic machinery

The scale-up procedure for hydraulic machinery consists in determining the amount of scalable losses of the investigated machine and then scaling up the performance data according to the variation of these losses. The scalable losses commonly coincide with the friction and leakage losses of the machine and vary at each operating point, according to the Reynolds number Re and the effect of surface roughness Ra. Quantifying them for each type of investigated machine at every operating point would be too time-consuming therefore international standards were introduced, which provide the ratio of scalable losses for each type of machine and the equations needed to calculate the performance scale-up.

Currently, there are two international standards describing how to conduct the scale-up process: the standard IEC 60193 published in 1999, and the more recent IEC 62097 issued in 2009. The accepted standards are two since the most recent one cannot be applied to all types of hydraulic machines, due to the lack of extensive studies. The limitations of the scale-up procedure of the older standard compared to the IEC 62097 standard are described in section 4.3.

4.1 IEC 60193 scale-up procedure

In the scale-up procedure according to the standard IEC 60193, the influence of surface roughness is not considered. It is therefore assumed that the scalable losses of each type of machine vary only with the Reynolds number Re. Figure 7 shows how the relative scalable losses δ, specified in equation (12), decrease with increasingly high Reynolds numbers, while the relative non-scalable losses, specified in equation (13), stay constant [5]. For instance, a pump model operating at a certain point with a Reynolds number Re_M, has a lower hydraulic efficiency than the full-size prototype, operating at the same point, but with a higher Reynolds number Re_P.

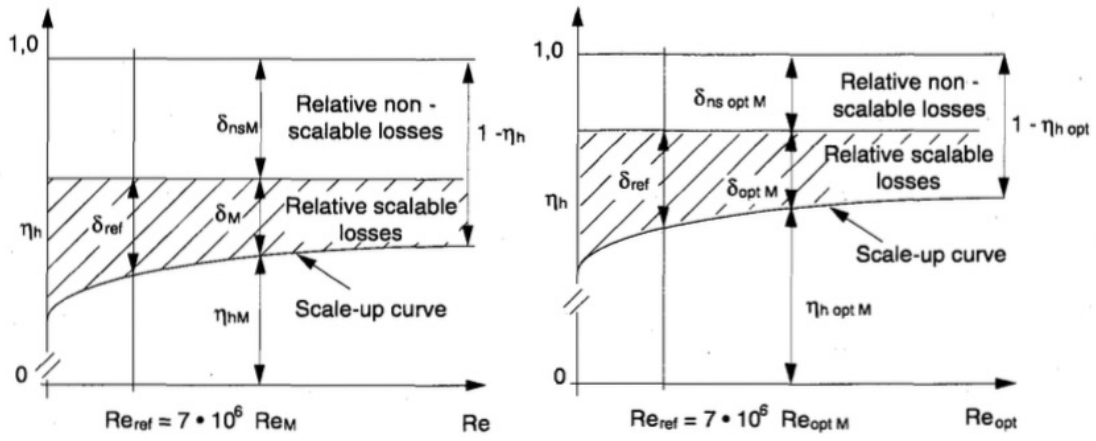

Figure 7: Variation of relative scalable losses [5].

Relative scalable and non-scalable losses according to IEC 60193 [5]:

$$\delta = (1 - \eta_h) \cdot V \tag{12}$$

$$\delta_{ns} = (1 - \eta_h) - \delta = (1 - \eta_h) \cdot (1 - V) \tag{13}$$

The coefficient V is the loss distribution coefficient and represents the ratio of relative scalable losses to relative total losses. It is a constant value, given in the standard for different types of hydraulic machines, for the point of optimum hydraulic efficiency at the reference Reynolds number $Re_{ref} = 7 \cdot 10^6$ [5].

The first step to scale up the efficiency from model to prototype consists in determining the relative scalable losses δ_{ref} at Re_{ref} with equation (14), where $\eta_{h,opt,M}$ stands for the hydraulic efficiency of the model at the optimum point and $Re_{opt,M}$ for the model Reynolds number at optimum efficiency. With the relative scalable losses and the Reynolds numbers of the model and the prototype at the investigated operation point, the efficiency difference $\Delta\eta_{h_{M->P}}$ at Re_{ref} can then be calculated with equation (15) [5].

$$\delta_{ref} = \frac{1 - \eta_{h,opt,M}}{\left[\left(\frac{Re_{ref}}{Re_{opt,M}}\right)^{0,16} + \frac{1-V_{ref}}{V_{ref}}\right]} \tag{14}$$

$$\Delta\eta_{h_{M->P}} = \delta_{ref} \cdot \left[\left(\frac{Re_{ref}}{Re_M}\right)^{0,16} - \left(\frac{Re_{ref}}{Re_P}\right)^{0,16}\right] \tag{15}$$

The prototype efficiency can then be determined by adding the efficiency difference to the model efficiency (equation (16)). The efficiency difference between model and prototype is associated, in this standard, with a decrease of mechanical power P_m. As shown in equation (17), the mechanical power ratio of prototype and model is directly proportional to the efficiency ratio [5].

$$\eta_{h,P} = \eta_{h,M} + \Delta\eta_{h_{M->P}} \tag{16}$$

$$\frac{P_{m,P}}{P_{m,M}} = \frac{\rho_P}{\rho_M} \cdot \left(\frac{D_P}{D_M}\right)^5 \cdot \left(\frac{n_P}{n_M}\right)^3 \cdot \frac{\eta_{h,P}}{\eta_{h,M}} \tag{17}$$

In reality, besides the mechanical power P_m, the scale-up effects affect also the specific hydraulic energy E_h and the discharge Q [5]. This simplification is one of the major limitations of this standard and got revised in the newer standard IEC 62097.

4.2 IEC 62097 scale-up procedure

The IEC 62097 standard utilizes a more specific approach to determine the efficiency scale-up for hydraulic machines, by dividing the investigated pump or turbine into its main components and analyzing the effects of scalable losses separately for each individual component. Pumps and turbines are therefore divided into the following

main parts [4]:

- spiral casing (SP)
- stay vanes (SV)
- guide vanes (GV)
- runner (RU)
- draft tube (DT)

Furthermore, the effects of the efficiency scale-up are considered to affect, not only the mechanical power P_m but also the specific hydraulic energy E and the discharge Q. The hydraulic efficiency difference $\Delta\eta_h$ between model and prototype is therefore split into the efficiency ratio Δ_T affecting the mechanical power P_m, the efficiency ratio Δ_E affecting the specific hydraulic energy E and the efficiency ratio Δ_Q affecting the discharge Q, all multiplied by the model hydraulic efficiency $\eta_{h,M}$ as shown in equation (18) [4].

$$\Delta\eta_h = \eta_{h,M} \cdot (\Delta_E + \Delta_T + \Delta_Q) \tag{18}$$

The hydraulic energy efficiency ratio Δ_E can be determined for each individual component of the investigated machine with equation (19). Δ_E depends upon the standardized reference scalable loss $\delta_{E,CO,ref}$ and the friction loss coefficients λ_{CO} of model, prototype and at reference Reynolds number Re_{ref} [4].

$$\Delta_{E,CO} = \delta_{E,CO,ref} \cdot \left(\frac{\lambda_{CO,M} - \lambda_{CO,P}}{\lambda_{CO,ref}} \right) \tag{19}$$

With the substitution of the friction coefficients with their explicit formulation, equation (19) assumes the form shown in equation (20). Δ_E now depends upon the Reynolds number Re, the wall roughness Ra, and the diameter D of model and

prototype, and also upon the velocity factor κ_u and the scalable hydraulic energy loss index $d_{E,CO,ref}$ [4].

$$\Delta_{E,CO} = d_{E,COref} \cdot \left[\left(4 \cdot 10^5 \cdot \kappa_{u,CO} \cdot \frac{Ra_{CO,M}}{D_M} + \frac{7 \cdot 10^6}{Re_M} \right)^{0,2} - \left(4 \cdot 10^5 \cdot \kappa_{u,CO} \cdot \frac{Ra_{CO,P}}{D_P} + \frac{7 \cdot 10^6}{Re_P} \right)^{0,2} \right] \tag{20}$$

The velocity factor $\kappa_{u,CO}$ is the ratio of the average relative flow velocity in each component v_{CO} against the peripheral velocity u (equation (21)). The scalable hydraulic energy loss index $d_{E,CO,ref}$ is defined in equation (24) by the reference scalable hydraulic energy loss $\delta_{E,CO,ref}$ (equation (23)) and the dimension factor $\kappa_{d,CO}$ (equation (22)). These values have been determined, in form of linear functions depending upon the specific speed N_{QE} at the best efficiency point, for every main component of each hydraulic machine type covered by this standard [4].

$$\kappa_{u,CO} = \frac{v_{CO}}{u} \tag{21}$$

$$\kappa_{d,CO} = \frac{d_{h,CO}}{D} \tag{22}$$

$$\delta_{E,CO,ref} = \frac{E_{Lf,CO,ref}}{E_{ref}} \tag{23}$$

$$d_{E,CO,ref} = \frac{\delta_{E,CO,ref}}{1 + 0,35 \cdot (\kappa_{u,CO} \cdot \kappa_{d,CO})^{0,2}} \tag{24}$$

To compute the efficiency ratio Δ_T a similar formula to the one used for Δ_E is proposed, with the dimension factor for the disc (relating to disc friction loss) κ_T and the scalable disc friction loss index $d_{T,ref}$, defined in equation (26) and (28) [4].

$$\Delta_T = d_{T,ref} \cdot \left[\left(7,5 \cdot 10^4 \cdot \kappa_T \cdot \frac{Ra_{T,M}}{D_M} + \frac{7 \cdot 10^6}{Re_M} \right)^{0,2} - \left(7,5 \cdot 10^4 \cdot \kappa_T \cdot \frac{Ra_{T,P}}{D_P} + \frac{7 \cdot 10^6}{Re_P} \right)^{0,2} \right] \tag{25}$$

$$\kappa_T = \frac{d_h}{D} \tag{26}$$

$$\delta_{T,ref} = \frac{P_{Ld,ref}}{P_{m,ref}} \tag{27}$$

$$d_{T,ref} = \frac{\delta_{T,ref}}{1 + 0,154 \cdot \kappa_T^{0,4}} \tag{28}$$

The efficiency ratio Δ_Q can generally be neglected if the seals of model and prototype are homologous. This is the case for the two reactor coolant pumps analyzed in this work. Otherwise, if the seals cannot be considered homologous, the scale-up process regarding the volumetric losses can be determined with the procedure presented in Annex E of the standard IEC 62097 [4].

With the efficiency ratios Δ_E, Δ_T and Δ_Q, it is then possible to calculate the scale-up of the hydraulic efficiency η_h, the specific hydraulic energy E, the mechanical power P_m, and the discharge Q, as shown for hydraulic machines working in pump operation in the equations (29), (30), (31), and (32) [4].

$$\eta_{h,P} = \eta_{h,M} \cdot (1 + \Delta_E) \cdot (1 + \Delta_T) \cdot (1 + \Delta_Q) \tag{29}$$

$$E_P = E_M \cdot \left(\frac{n_P}{n_M}\right)^2 \cdot \left(\frac{D_P}{D_M}\right)^2 \cdot (1 + \Delta_E) \tag{30}$$

$$P_{m,P} = P_{m,M} \cdot \frac{\rho_P}{\rho_M} \cdot \left(\frac{n_P}{n_M}\right)^3 \cdot \left(\frac{D_P}{D_M}\right)^5 \cdot \frac{1}{1 + \Delta_T} \tag{31}$$

$$Q_P = Q_M \cdot \frac{n_P}{n_M} \cdot \left(\frac{D_P}{D_M}\right)^3 \cdot (1 + \Delta_Q) \tag{32}$$

4.3 Performance scale-up for RCP and its current limitations

Reactor coolant pumps are part of the hydraulic machines excluded from the standard IEC 62097 and therefore still follow the guidelines of the standard IEC 60193 with its limitations. One of the main reasons why the new standard was introduced in the first place, is that with the method of the older standard machines with lower design quality get a larger scale-up value than machines with more efficient designs, despite the fact that the increased losses of less efficient designs are mainly non-scalable losses. Furthermore, the procedure overestimates the efficiency increase of hydraulic machines with low efficiencies or unfavorable flow dynamics in their components (as the cylindrical RCP casing), due to the inaccuracies and simplifications listed below [4]:

- The use of a constant loss distribution factor V_{ref} for each type of pump regardless of its individual design quality
- The loss distribution factor V_{ref} is a constant value and therefore does not consider the influence of specific speed
- The variation of the scalable losses depends only on the variation of the Reynolds number
- The scale-up formula assumes smooth surfaces for model and prototype

- The sole association of efficiency scale-up effects to a decrease of mechanical power P_m of the pump, instead of considering multiple scale-up factors and assigning each accordingly either to the specific hydraulic energy E, the discharge Q or the mechanical power P_m

Regarding the last point, it can be assumed that the efficiency scale-up effects of the axial Type 1134 RCP can be exclusively associated with a loss of specific energy E since the blade tip friction and volumetric losses are negligible. On the other hand, the Type 1400 pump has a shroud ring and its friction is not negligible, therefore, the effects of those losses have to be associated with a decrease of mechanical power P_m. The seals of model and prototype are homologous, hence, also for this RCP, the volumetric losses are negligible. Considering these facts, it is clear, that a sole decrease of mechanical power P_m, as assumed in the standard IEC 60193, does not reflect the real behavior of RCPs. Being able to apply new standard IEC 62097 would definitely improve the scale-up procedure in these regards, as it would be possible to correctly assign the scale-up effects to the specific hydraulic energy E, the discharge Q, and the mechanical power P_m.

Former step-up calculations for the two pumps, following the IEC 60193 standard, show an efficiency increase between model and prototype of roughly 5% [1]. In the following chapters, the scale-up factors necessary to calculate a performance scale-up with the new standard will be determined, so that in chapter 7.3, a comparison and evaluation of the results between the two standards can be made.

5 IEC 62097 scale-up procedure adapted to RCPs

As mentioned in chapter 4.3, reactor coolant pumps are currently not covered by the international standard IEC 62097, since the scale-up factors given in standard are not applicable to RCPs. It is therefore essential to determine these factors for the main RCP components, to be able to employ the standard. In the following chapters, the scale-up factors are going to be determined for the two investigated RCPs, while in Appendix A the calculation, performed with the software *Mathcad Prime* for the Type 1134 RCP, is presented.

5.1 Determination of scale-up factors for RCPs

The IEC 62097 scale-up equations in chapter 4.2 contain four different factors, which are given by the IEC 62097 standard according to the specific speed of the machine at the best efficiency point:

- The velocity factor κ_u, defined by equation (21)
- The dimension factor κ_d, defined by equation (22) and (26)
- The reference scalable energy loss δ_{ref}, defined by equation (23) and (27)
- The scalable energy loss index d_{ref}, defined by equation (24) and (28)

As shown by the equations, to determine the velocity factor κ_u it is necessary to calculate the mean flow velocity v in each component and divide it by the peripheral velocity u of the runner. The dimension factor κ_d can be obtained through the geometry of the model, as it is the ratio of the hydraulic diameter d_h of the component to the reference diameter D of the machine. For the scalable hydraulic energy loss δ, the friction losses E_{Lf} have to determined in each component and divided by the specific hydraulic energy E_h, except for the disk friction losses P_{Ld}, which have to be divided by the mechanical power P_m of the machine. The scalable energy loss index d_{ref} is a function depending upon the other scale-up factors and

can be determined by the above-mentioned equations. To convert these factors into linear functions of the specific speed N_{QE} of the machine at the best efficiency point, they have to be determined for multiple RCPs (at least two) at the best efficiency point and plotted according to the specific speed. In the following sections, this procedure is conducted for the two axial working RCPs presented in chapter 2.1. For the study, the pumps have been divided into the following main components, shown in Figure 8 and 9:

- Runner (RU)
  - Runner blades (RB)
  - Annular runner channel (RUC)
- Guide vane section (GVS)
  - Guide vanes (GV)
  - Annular guide vane channel (GVC)
- Cylindrical casing (CY)
- Shroud ring (SR) (only the Type 1400 RCP has a shroud ring)

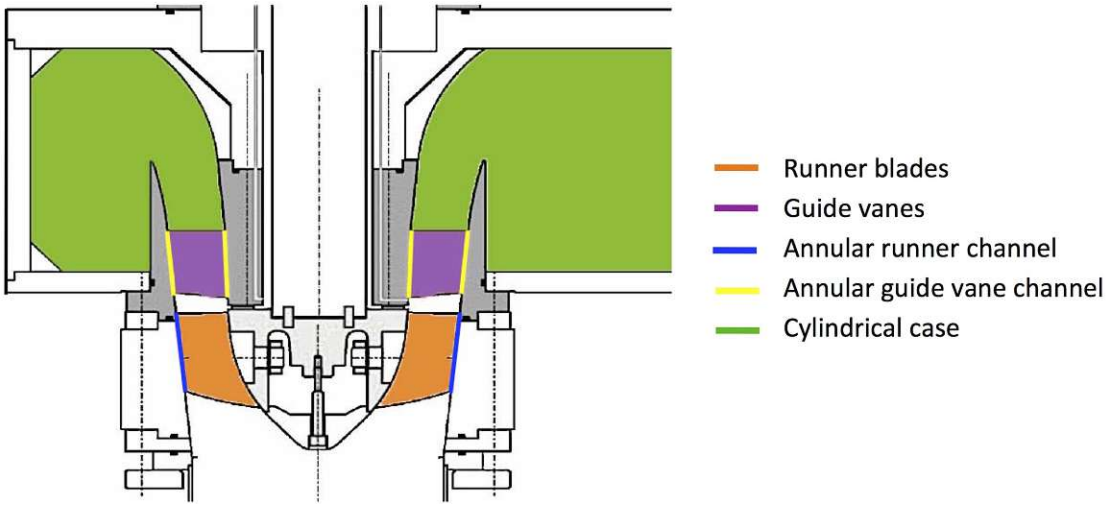

Figure 8: Components subdivision for the Type 1134 RCP

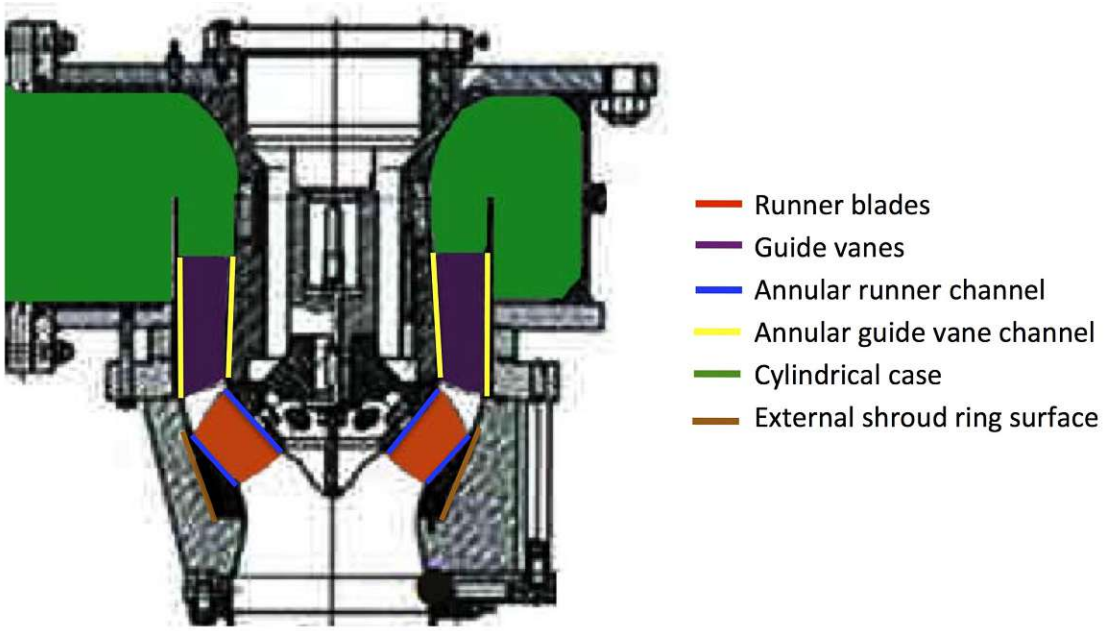

Figure 9: Components subdivision for the Type 1400 RCP

As shown in the figures above, only the Type 1400 RCP has a shroud ring connected to the external edge of the runner blades. On the internal surface, the ring generates friction losses which affect the specific hydraulic energy E of the pump, and on the outside surface, losses like those generated by two concentric rotating cylinders, which affect the mechanical power P_m. The Type 1134 RCP, on the other hand, does not have the shroud ring and therefore generates fewer friction losses affecting the mechanical power P_m, as the surface area of the blade ends is much smaller than the surface area of the Type 1400 shroud ring. For this reason, the losses affecting the mechanical power are negligible for the Type 1134 RCP. Furthermore, the friction losses in the annular casing section of the Type 1134 pump can't be determined like for a flow through an annular channel, since the internal surface area of the annulus rotates with the runner velocity, while the outside surface is stationary. To avoid further subdivisions and since the area of the internal section of the annular channel is much smaller than the area at the outside diameter, the friction losses of the internal surface have not been considered in this study. The annular runner channel of the Type 1400 pump does not have this issue since,

with the shroud ring connected to the runner blades, both the inner and the outer surface of the annular channel rotate with the same peripheral velocity u.

5.2 The investigated operating points and RCP data

The scale-up factors for the two RCPs have to be determined at the best efficiency point. The performance data at best efficiency was selected among the test-results described in chapter 3 and converted from the measured shaft speed to the constant shaft speed of 1450 rpm, for the Type 1134 RCP model and 1000 rpm, for the Type 1400 RCP model. Table 1 shows the main model performance data necessary to the determination of the scale-up factors for the two pumps, Table 2 the operating conditions at the best efficiency point for the constant shaft speed, while Table 3 indicates the wall roughness of each component.

		Type 1134 RCP	Type 1400 RCP
$\mathbf{D}_M$	[m]	0,29777	0,36348
$\mathbf{n}_M$	[rpm]	1450	1000
$\mathbf{Re}_M$	[-]	6707519	6892721
$\mathbf{Q}_M$	$[\frac{m^3}{s}]$	0,24344	0,3984
$\mathbf{E}_{h,M}$	$[\frac{m^2}{s^2}]$	130,353	149,955
$\mathbf{P}_{m,M}$	[W]	38263,8	72355,3
$\boldsymbol{\eta}_{h,M}$	[%]	0,82783	0,82419

Table 1: Operating data of the two investigated RCP models [1]

	$\boldsymbol{\rho}_{W,M}$	$\mathbf{p}_{amb,M}$	$\mathbf{t}_{W,M}$	$\mathbf{g}_M$
	$[\frac{kg}{m^3}]$	$[Pa]$	$[°C]$	$[\frac{m}{s^2}]$
Type 1134 RCP	998,2	101325	20	9,80703
Type 1400 RCP	998,2	101325	20	9,80703

Table 2: Operating conditions of the two investigated RCP models [1]

	$\mathbf{Ra}_{RB}$	$\mathbf{Ra}_{GV}$	$\mathbf{Ra}_{RUC}$	$\mathbf{Ra}_{GVC}$	$\mathbf{Ra}_{CY}$
	$[\mu m]$	$[\mu m]$	$[\mu m]$	$[\mu m]$	$[\mu m]$
Type 1134 RCP	0,5	0,5	0,8	2	2
Type 1400 RCP	0,5	0,5	0,8	2	2

Table 3: Wall roughness of each investigated RCP component [1]

5.3 Scale-up factors for the runner

The runner scale-up factors are determined by separately calculating the friction losses of the runner blades and those of the annular runner channel, and then combining the results to obtain the factors for the whole runner.

5.3.1 Runner blades friction losses

The runner blades friction losses of the two RCP models are defined, by considering the flow through the runner as a flow over Z_{RB} flat plates, where Z_{RB} stands for the number of runner blades, indicated in Table 10. With this simplification, it is possible to estimate the friction factor $C_{f,RB}$ of the blades with the explicit friction

factor formula for flat plates, provided by the standard IEC 62097 [4]. If the suction and pressure side of the blades is not considered separately, the energy loss due to friction $E_{Lf,RB}$ can be determined through equation (35), with $N = 2 \cdot Z_{RB}$ (two sides for each blade). In this case, the average relative velocity for the whole blade is used. If the velocity profile along the suction and pressure side of the blades is given, equation (35) with $N = Z_{RB}$ is applied once for the pressure side and once for the suction side of the blades. The resulted energy losses are then added into one value. Regarding the studied RCPs, equation (35) with $N = 2 \cdot Z_{RB}$ is utilized for the Type 1400 RCP, while the version with $N = Z_{RB}$ is applied to the suction and pressure sides of the Type 1134 RCP blades. The different approach is necessary since the velocity distribution along the blades pressure and suction sides is known only for the Type 1134 RCP, from CFD-simulations carried out by *ANDRITZ AG*. Equation (35) is obtained by substituting the friction force F_f, defined in equation (33) [7], into equation (34), and multiplying the equation by N blade surfaces. L_{RB} is the length of one blade, B_{RB} the width, and $\frac{A_{RB}}{Z_{RB}}$ the sectional area of the flow for one blade, while w stands for the average flow velocity relative to the blade, which is moving at the peripheral velocity u.

$$F_f = C_f \cdot \left(\rho \cdot \frac{v^2}{2} \right) \cdot S_0 \tag{33}$$

with S_0 = flat plate surface = $L_{RU} \cdot B_{RU}$

$$E_{Lf} = \frac{\Delta p}{\rho} = \frac{F_f}{A \cdot \rho} \tag{34}$$

with A = sectional area of the flow for one blade = $\frac{A_{RU}}{Z_{RU}}$

$$E_{Lf,RB} = C_{f,RB} \cdot \frac{L_{RB} \cdot B_{RB}}{\frac{A_{RU}}{Z_{RB}}} \cdot \frac{w^2}{2} \cdot N \tag{35}$$

with A_{RU} = sectional area of the flow of the annular runner channel and
N = number of blade surfaces

The mean relative flow velocity w is obtained by calculating and then averaging the relative flow velocities at the internal and external blade diameter for the inlet and outlet, as indicated in Figure 10. The peripheral runner velocity u at the four points is determined through equation (36), the absolute peripheral velocity of the flow c_u with Euler's equation (37) [7], and the absolute meridian velocity c_m through the discharge with equation (38).

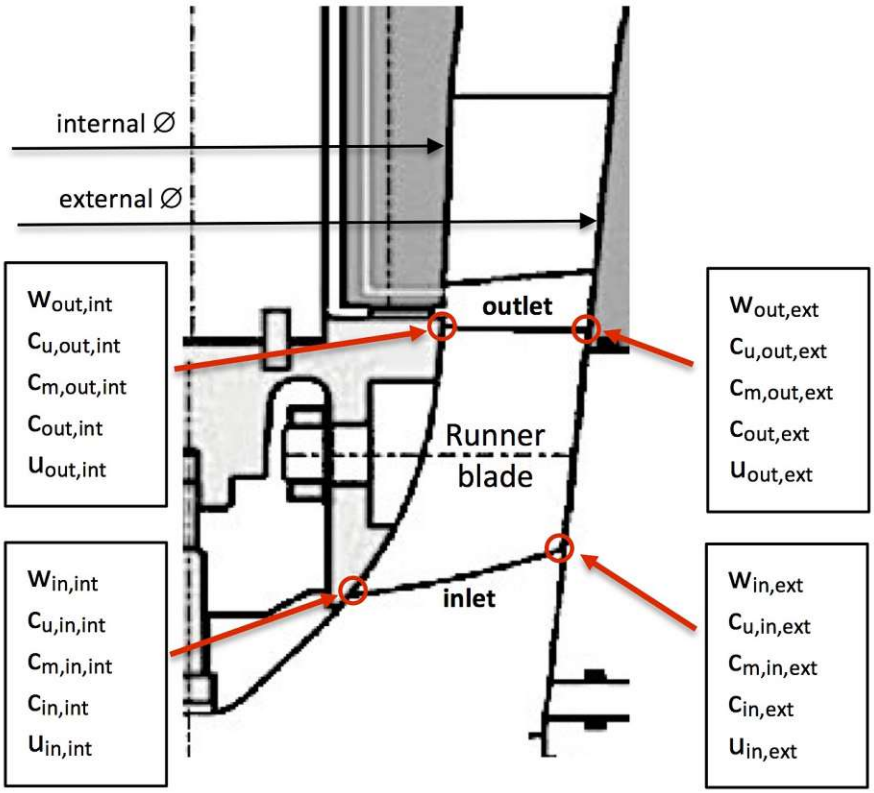

Figure 10: Flow velocities in runner blades

$$u = 2 \cdot \pi \cdot n_M \cdot \frac{D_{RU}}{2} \tag{36}$$

$$c_u = \frac{g \cdot H_M}{u} \cdot \frac{1}{\eta_{h,M}} \tag{37}$$

$$c_m = \frac{Q_M}{A_{RU}} \tag{38}$$

The absolute flow velocity c can then be determined from the axial and peripheral component with equation (39), by considering the velocity triangles of the pump blades depicted in Figure (11).

$$c = \sqrt{c_m^2 + c_u^2} \tag{39}$$

At the inlet, the peripheral component c_u is equal to zero since the incoming flow is considered to be purely axial. Consequently, at the inlet, the absolute flow velocity coincides with the axial component.

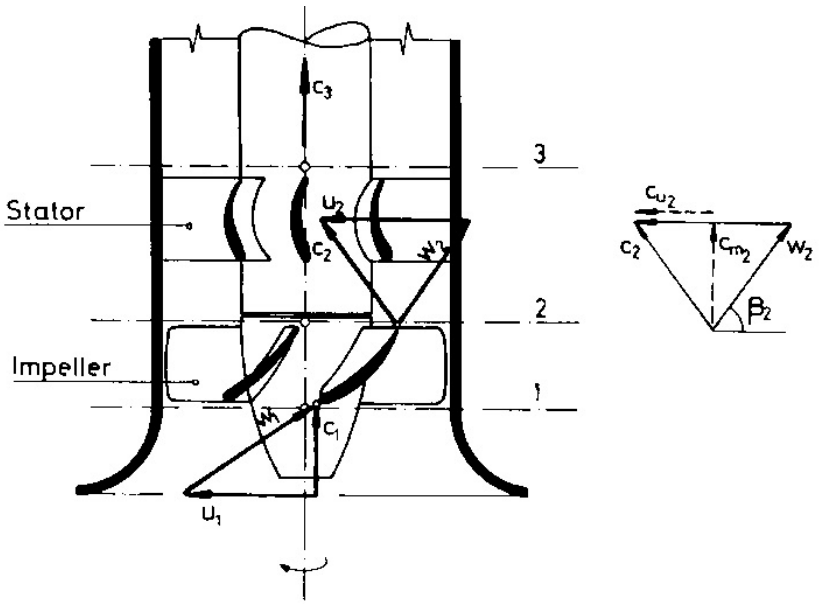

Figure 11: Velocity triangles of an axial flow pump [6]

The angle of the relative flow velocity for each point can be determined through the geometric relations of the velocity triangles, with equation (40). By inserting the angle β in equation (41), the relative flow velocities at each blade point are obtained so that, by averaging them in equation (42), the mean relative flow velocity in the runner w can be determined.

$$\beta = \arctan \frac{c_m}{u - c_u} \tag{40}$$

$$w_{point} = \frac{c_m}{\sin \beta} \tag{41}$$

$$w = \frac{w_{in,int} + w_{in,ext} + w_{out,int} + w_{out,ext}}{4} \tag{42}$$

The velocities resulted from the above-described calculations are shown in Table 4, 5, and 6, while Table 7 indicates the average relative flow velocity of the Type 1134 RCP suction and pressure side of the blades. These values were obtained by averaging the velocity distribution along the blade sides, provided by *ANDRITZ AG* [1].

	$\boldsymbol{u}_{in,int}$	$\boldsymbol{u}_{in,ext}$	$\boldsymbol{u}_{out,int}$	$\boldsymbol{u}_{out,ext}$
	$[\frac{m}{s}]$	$[\frac{m}{s}]$	$[\frac{m}{s}]$	$[\frac{m}{s}]$
Type 1134 RCP	8,989	21,699	15,033	23,515
Type 1400 RCP	8,378	15,708	17,069	21,991

Table 4: Peripheral inlet and outlet blade velocity at the internal and external diameter of the runner

	$\boldsymbol{c}_{in,int}$	$\boldsymbol{c}_{in,ext}$	$\boldsymbol{c}_{out,int}$	$\boldsymbol{c}_{out,ext}$
	$[\frac{m}{s}]$	$[\frac{m}{s}]$	$[\frac{m}{s}]$	$[\frac{m}{s}]$
Type 1134 RCP	4,580	4,580	11,814	8,642
Type 1400 RCP	6,064	6,064	11,525	9,363

Table 5: Absolute inlet and outlet flow velocity at the internal and external diameter of the runner

	$\boldsymbol{w}_{in,int}$	$\boldsymbol{w}_{in,ext}$	$\boldsymbol{w}_{out,int}$	$\boldsymbol{w}_{out,ext}$	$\boldsymbol{w}$ [average]
	$[\frac{m}{s}]$	$[\frac{m}{s}]$	$[\frac{m}{s}]$	$[\frac{m}{s}]$	$[\frac{m}{s}]$
Type 1134 RCP	10,089	22,177	7,115	17,684	14,266
Type 1400 RCP	10,342	16,838	7,766	14,401	12,337

Table 6: Relative inlet and outlet flow velocity at the internal and external diameter, and mean relative flow velocity of the runner

	$\boldsymbol{w}_{\mathrm{PS}}$	$\boldsymbol{w}_{\mathrm{SS}}$
	$[\frac{m}{s}]$	$[\frac{m}{s}]$
Type 1134 RCP	11,207	15,460

Table 7: Average relative flow velocity of the runner blades pressure side (PS) and suction side (SS) of the Type 1134 RCP [1]

Once the mean relative flow velocity w is determined, it is possible to define the scale-up factors for the component. The dimension factor $\kappa_{d,RU}$ and the velocity factor $\kappa_{u,RU}$, shown in Table 8, are obtained through equation (43) and (44) [4].

$$\kappa_{d,RU} = \frac{L_{RU}}{D_M} \tag{43}$$

with L_{RU} = blade length and D_M = reference diameter of the RCP model

$$\kappa_{u,RU} = \frac{w}{u} \tag{44}$$

with u = peripheral velocity at reference diameter

	$\kappa_{d,RU}$	$\kappa_{u,RU}$
	[-]	[-]
Type 1134 RCP	0,73883	0,63106
Type 1400 RCP	0,55024	0,64822

Table 8: Dimension factor and velocity factor for the runner blades of the studied RCPs

With these two factors, it is possible to compute the friction loss factor $C_{f,RB}$, defined in equation (45), according to the standard IEC 62097, and with equation (35) the specific hydraulic energy loss due to friction $E_{Lf,RB}$ can be determined [4].

For the Type 1134 RCP, a separate calculation of $E_{Lf,RB}$ for the pressure side and the suction side is performed. To do so, the velocity factor and the friction coefficient, inserted in equation (35), are calculated with the average relative flow velocities for each side indicated in Table 7. The hydraulic energy loss of each blade side is then added and presented in Table 10 as the total energy loss due to friction of the Type 1134 RCP runner blades. The results of the specific calculation of $E_{Lf,RB}$ of each blade side are shown in Table 9, while the total results for both pumps are presented in Table 10.

$$C_{f,RB} = 0.0032 \cdot \left(0.8 \cdot \left(5 \cdot 10^5 \cdot \frac{Ra_{RB}}{L_{RB}} + \frac{Re_{ref}}{\kappa_{d,RU} \cdot \kappa_{u,RU} \cdot Re_M} \right)^{0.2} + 0.2 \right) \quad (45)$$

$$C_{f,RB,ref} = 0.0032 \cdot \left(0.8 \cdot \left(\frac{1}{\kappa_{d,RU} \cdot \kappa_{u,RU}} \right)^{0.2} + 0.2 \right) \quad (46)$$

(Simplified version of equation (45), since it represents the model with smooth surface -> $Ra = 0$ and at reference Reynolds number -> $Re_M = Re_{ref}$)

Type 1134 RCP	$\boldsymbol{\kappa_{u,RU^*}}$	C_{f,RB^*}	E_{Lf,RB^*}
	[-]	[-]	$[\frac{m^2}{s^2}]$
Pressure side	0,49572	0,00402	1,986
Suction side	0,68387	0,00387	3,644

Table 9: Velocity factors, friction coefficients, and total specific energy loss due to friction for pressure and suction side of the Type 1134 RCP runner blades

	$\boldsymbol{Z_{RB}}$ [number of blades]	$\boldsymbol{C_{f,RB}}$	$\boldsymbol{C_{f,RB,ref}}$	$\boldsymbol{E_{Lf,RB}}$
	[-]	[-]	[-]	$[\frac{m^2}{s^2}]$
Type 1134 RCP	5	0,00391	0,00362	5,630
Type 1400 RCP	6	0,00403	0,00379	4,917

Table 10: Number of blades, friction coefficients, and total specific energy loss due to friction for the runner blades of the studied RCPs

5.3.2 Annular runner channel friction losses

The annular runner channel of the Type 1134 RCP differs from the one of the Type 1400 RCP since the runner does not have a shroud ring connected to the blade tips. This implies that the relevant velocity of the stationary surface at the outer diameter differs from the relevant velocity of the surface at the inner diameter, which is rotating at the rotational speed of the runner. For this reason, it is not possible to determine the scale-up factors for the whole component and a further split up would be necessary. To avoid an additional component break-up only the outer surface of the annular channel is considered, since the influence of the inner surface, by being considerably smaller than the outer surface, is negligible. On the other hand, the Type 1400 RCP does not display this issue, since both the inner and the outer surface of the annular channel rotate with the same rotational speed of the runner. For the reasons mentioned above, the flow in the annular runner channel of the Type 1134 pump is modeled as a flow through a straight pipe, while for the Type 1400 pump it is modeled as flow through a straight annular channel.

The dimension factor $\kappa_{d,RUC}$ is defined in equation (50), as the hydraulic diameter d_h of the channel divided by the reference diameter D_M of the pump. For the Type 1134 pump channel, being modeled as a pipe, the hydraulic diameter coincides with the reference diameter, while for the Type 1400 pump the hydraulic diameter of the annular channel is determined through equation (49) [12]. The velocity factor $\kappa_{u,RUC}$ is defined by equation (48), where, for the Type 1134 RCP, the mean velocity v_{RUC} is determined by averaging the absolute flow velocities of the runner at the external diameter of the inlet and outlet (equation (47)), while for the Type 1400 RCP, the mean velocity is equal to the average relative flow velocity w in the runner. The hydraulic diameters, mean velocities, dimension and velocity factors of the two RCPs are shown in Table 11.

$$v_{RUC,\text{Type 1134}} = \frac{c_{in,ext} + c_{out,ext}}{2} \tag{47}$$

$$\kappa_{u,RUC} = \frac{v_{RUC}}{u} \tag{48}$$

$$d_h = \frac{4 \cdot A}{P} \tag{49}$$

with $A = A_{RUC}$ = sectional area of the flow in the annular channel and
$P = P_{RUC}$ = wetted channel perimeter

$$\kappa_{d,RUC} = \frac{d_{h,RUC}}{D_M} \tag{50}$$

	$\boldsymbol{d_{h,RUC}}$	$\boldsymbol{\kappa_{d,RUC}}$	$\boldsymbol{v_{RUC}}$	$\boldsymbol{\kappa_{u,RUC}}$
	$[m]$	[-]	$[\frac{m}{s}]$	[-]
Type 1134 RCP	0,29777	1	6,611	0,292
Type 1400 RCP	0,16531	0,455	12,337	0,64822

Table 11: Hydraulic diameter, dimension factor, mean velocity and velocity factor for the annular runner channel of the studied RCPs

The friction loss coefficients at operating and reference condition λ_{RUC} and $\lambda_{RUC,ref}$ are obtained through the explicit formulation of the Colebrook formula for pipe friction, proposed by Nichtawitz (equation (51) and (52) [4]). With the friction coefficients λ_{RUC} and $\lambda_{RUC,ref}$ and the mean flow velocity in the channel v_{RUC}, the specific hydraulic energy loss $E_{Lf,RUC}$ due to friction can be determined through equation (54) [4]. In the equation for the Type 1400 RCP, the channel length L_{RUC} is equal to the runner blade length, while for the Type 1134 RCP, since the channel wall is stationary, L_{RUC} is equal to the distance traveled by a fluid particle along the pipe surface. The distance $L_{RUC,Type1134}$ is defined in equation (53) as the hypotenuse of the triangle, having length equal to the peripheral distance traveled

by the particle $L_{RUC,u}$ and height equal to the traveled axial distance $L_{RUC,m}$. $L_{RUC,m}$ is equal to the axial length of the runner channel, while $L_{RUC,u}$ can easily be determined by multiplying the absolute peripheral flow velocity c_u with the time t needed by a particle to cover the axial distance ($t = \frac{L_{RUC,m}}{c_m}$).

$$\lambda_{RUC} = 0.0085 \left(0.74 \left(4 \cdot 10^5 \frac{Ra_{RUC}}{\kappa_{d,RUC} \cdot D_M} + \frac{Re_{ref}}{\kappa_{d,RUC} \cdot \kappa_{u,RUC} \cdot Re_M} \right)^{0.2} + 0.26 \right) \quad (51)$$

$$\lambda_{RUC,ref} = 0.0085 \cdot \left(0.74 \cdot \left(\frac{1}{\kappa_{d,RUC} \cdot \kappa_{u,RUC}} \right)^{0.2} + 0.26 \right) \quad (52)$$

(simplified version of equation (51), since it represents the model with smooth surface -> $Ra = 0$ and at reference Reynolds number -> $Re_M = Re_{ref}$)

$$L_{RUC,Type1134} = \sqrt{L_{RUC,u}^2 + L_{RUC,m}^2} \quad (53)$$

$$E_{Lf,RUC} = \lambda_{RUC} \cdot \frac{L_{RUC}}{d_{h,RUC}} \cdot \frac{v_{RUC}^2}{2} \quad (54)$$

The results for the friction coefficients λ_{RUC} and $\lambda_{RUC,ref}$ and the specific hydraulic energy loss due to friction $E_{Lf,RUC}$ are shown in Table 12.

	$\boldsymbol{\lambda_{RUC}}$	$\boldsymbol{\lambda_{RUC,ref}}$	$\boldsymbol{E_{Lf,RUC}}$
	[-]	[-]	$[\frac{m^2}{s^2}]$
Type 1134 RCP	0,0108	0,0103	0,1080
Type 1400 RCP	0,0110	0,0102	1,0142

Table 12: Friction coefficients, and specific energy loss due to friction for the annular runner channel of the studied RCPs

5.3.3 Runner scale-up factors

Once the specific energy friction losses of the runner blades and the annular channel are obtained, the scale-up factors for the whole runner can be determined. The relative scalable hydraulic energy loss $\delta_{E,RU}$ is defined in equation (56) as the ratio of the specific hydraulic energy loss due to friction $E_{Lf,RU}$ of the runner, to the specific hydraulic energy $E_{h,M}$ of the model. $E_{Lf,RU}$, indicated in Table 13, is equal to the sum of the blade losses $E_{Lf,RB}$ and the annular channel losses $E_{Lf,RUC}$ (equation (55)).

The calculated relative scalable hydraulic energy loss $\delta_{E,RU}$ represents the model behavior at its current Reynolds number and its wall roughness. To be able to apply $\delta_{E,RU}$ to all axial flow RCPs, it is first necessary to convert the factor to a model with the reference Reynolds number $Re_{ref} = 7 \cdot 10^6$ and smooth surface. This is achieved by multiplying $\delta_{E,RU}$ with the ratio of the friction factors $C_{f,RU,ref}$ and $C_{f,RU}$ (equation (57)), where $C_{f,RU,ref}$ is the friction factor for the model at reference Reynolds number and smooth surfaces (equation (46)). Since the dominating losses are those of the runner blades, the friction factors $C_{f,RU,ref}$ and $C_{f,RU}$ of the runner are set equal to $C_{f,RB,ref}$ and $C_{f,RB}$, determined for the runner blades. The same is done for the dimension factor $\kappa_{d,RU}$ and the velocity factor $\kappa_{u,RU}$, which are utilized to determine the scalable hydraulic energy loss index $d_{E,RU,ref}$ in equation (58) [4]. The dimension factor $\kappa_{d,RU}$, the velocity factor $\kappa_{u,RU}$, and the specific energy loss due to friction $E_{Lf,RU}$ of the runner are presented in Table 13, while the relative and reference scalable hydraulic energy loss $\delta_{E,RU}$ and $\delta_{E,RU,ref}$, and the scalable hydraulic energy loss index $d_{E,RU,ref}$ are indicated in Table 14.

$$E_{Lf,RU} = E_{Lf,RB} + E_{Lf,RUC} \tag{55}$$

$$\delta_{E,RU} = \frac{E_{Lf,RU}}{E_{h,M}} \tag{56}$$

$$\delta_{E,RU,ref} = \frac{C_{f,RU,ref}}{C_{f,RU}} \tag{57}$$

$$d_{E,RU,ref} = \frac{\delta_{E,RU,ref}}{1 + 0.25 \cdot (\kappa_{u,RU} \cdot \kappa_{d,RU})^{0.2}} \tag{58}$$

	$\boldsymbol{\kappa_{d,RU}}$	$\boldsymbol{\kappa_{u,RU}}$	$\boldsymbol{E_{Lf,RU}}$
	[-]	[-]	$[\frac{m^2}{s^2}]$
Type 1134 RCP	0,73883	0,63106	5,738
Type 1400 RCP	0,55024	0,64822	5,931

Table 13: Dimension factor, velocity factor, and specific energy loss due to friction for the runner of the studied RCPs

	$\boldsymbol{\delta_{E,RU}}$	$\boldsymbol{\delta_{E,RU,ref}}$	$\boldsymbol{d_{E,RU,ref}}$
	[-]	[-]	[-]
Type 1134 RCP	0,0440	0,0408	0,0336
Type 1400 RCP	0,0396	0,0371	0,0308

Table 14: Relative and reference scalable hydraulic energy loss, and scalable hydraulic energy loss index for the runner of the studied RCPs

5.4 Scale-up factors for the guide vane section

The scale-up factors for the guide vane section are determined, as for the runner, by separately calculating the friction losses of the guide vanes and those of the annular guide vane channel, and then combining the results to obtain the factors for the whole section.

5.4.1 Guide vanes friction losses

The friction losses of the guide vanes can be determined with the same equations utilized for the runner blades. What changes, other than the geometry, are the velocities. As the guide vanes aren't rotating, the relevant velocity to determine the friction losses and the velocity factor is the mean flow velocity v_{GV}, obtained by averaging the velocities of the four points shown in Figure 12. At the guide vane inlet, the velocity $v_{GV,in}$ is considered to be equal to the absolute flow velocity c_{out} at the runner outlet (equation (59)). The velocity $v_{GV,out}$ at the guide vane outlet, on the other hand, is determined through the discharge Q with equation (60), since the flow is now purely axial. The velocities are then averaged in equation (61), to obtain the mean flow velocity v_{GV}. The calculated velocities are presented in Table 15.

$$v_{GV,in} = \frac{c_{out,int} + c_{out,ext}}{2} \tag{59}$$

$$v_{GV,out} = \frac{Q_M}{A_{GV,out}} \tag{60}$$

with $A_{GV,out}$ = sectional area of the flow of the annular guide vane channel outlet

$$v_{GV} = \frac{v_{GV,in} + v_{GV,out}}{2} \tag{61}$$

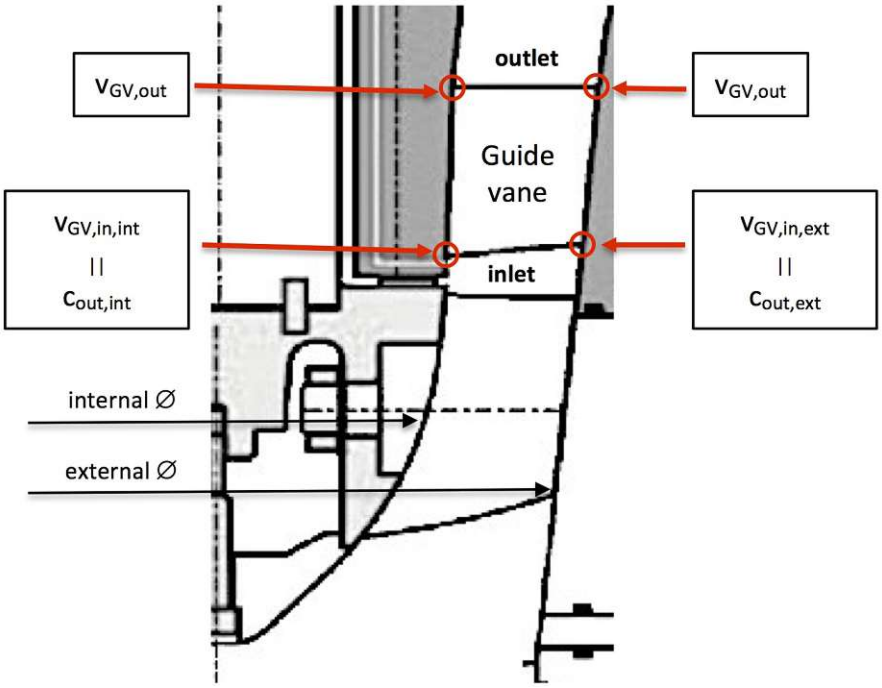

Figure 12: Flow velocities in the guide vanes

	$v_{GV,in}$	$v_{GV,out}$	v_{GV} [average]
	$[\frac{m}{s}]$	$[\frac{m}{s}]$	$[\frac{m}{s}]$
Type 1134 RCP	10,228	4,648	7,438
Type 1400 RCP	10,444	3,862	7,153

Table 15: Inlet, outlet and mean flow velocity for the guide vanes

The dimension factor $\kappa_{d,GV}$ and the velocity factor $\kappa_{u,GV}$ can then be determined by substituting the runner blade length L_{RU} with the guide vane length L_{GV} in equation (43), and the mean relative flow velocity in the runner w_{RU} with the mean flow velocity of the guide vane v_{GV} in equation (44).

	$\kappa_{d,GV}$	$\kappa_{u,GV}$
	[-]	[-]
Type 1134 RCP	0,30225	0,32901
Type 1400 RCP	0,66324	0,37586

Table 16: Dimension factor and velocity factor for the guide vanes

As for the runner blades, the energy loss due to friction $E_{Lf,GV}$ of the Type 1134 RCP can be separately calculated for the pressure and suction side of the guide vanes, since the velocity distribution along the vanes is known from CFD-simulations carried out by *ANDRITZ AG*. The average guide vane velocity for the pressure and suction side is indicated in Table 17 [1]. With the average velocity for each side, the velocity factor κ_{u,GV^*} and the friction factor C_{f,GV^*}, necessary to determine the energy loss due to friction E_{Lf,GV^*} for each side, can be calculated by inserting the guide vane data into equation (44) and (45). The results are presented in Table 18, together with the energy loss due to friction E_{Lf,GV^*}, obtained through equation (62) with $N = Z_{GV}$.

$$E_{Lf,GV} = C_{f,GV} \cdot \frac{L_{GV} \cdot B_{GV}}{\frac{A_{GV}}{Z_{GV}}} \cdot \frac{v_{GV}^2}{2} \cdot N \tag{62}$$

with A_{GV} = sectional area of the flow of the annular guide vane channel and
N = number of vane surfaces

	$v_{GV\mathrm{PS}}$	$v_{GV\mathrm{SS}}$
	$[\frac{m}{s}]$	$[\frac{m}{s}]$
Type 1134 RCP	5,457	7,949

Table 17: Average flow velocity of the guide vanes pressure side (PS) and suction side (SS) of the Type 1134 RCP [1]

Type 1134 RCP	$\kappa_{u,GV*}$	$C_{f,GV*}$	$E_{Lf,GV*}$
	[-]	[-]	$[\frac{m^2}{s^2}]$
Pressure side	0,24139	0,00516	1,649
Suction side	0,3516	0,00489	3,318

Table 18: Velocity factors, friction coefficients, and total specific energy loss due to friction for pressure and suction side of the Type 1134 RCP guide vanes

The energy loss due to friction $E_{Lf,GV}$ of the Type 1400 RCP, indicated in Table 19, is determined with equation (62), with $N = 2 \cdot Z_{GV}$. The value of $E_{Lf,GV}$ for the Type 1134 RCP in Table 19 is obtained by making the sum of the specific energy loss of the suction and pressure side of the guide vanes (Table 18). Table 19 shows also the friction factors $C_{f,GV}$ and $C_{f,GV,ref}$ of the two pumps, which were obtained by inserting the average guide vane flow velocity (Table 15) into equation (45) and (46), adapted to guide vanes.

	Z_{GV} [number of blades]	$C_{f,GV}$	$C_{f,GV,ref}$	$E_{Lf,GV}$
	[-]	[-]	[-]	$[\frac{m^2}{s^2}]$
Type 1134 RCP	14	0,00493	0,00470	4,967
Type 1400 RCP	11	0,00419	0,00402	4,999

Table 19: Number of blades, friction coefficients, and specific energy loss due to friction for the guide vanes of the studied RCPs

5.4.2 Annular guide vane channel friction losses

The friction losses for the annular guide vane channel are determined with the same equations utilized for the annular runner channel. The annular section, being stationary in both machines, is modeled as a straight annular channel, having length L_{GVC} equal to the length L_{GV} of the guide vanes. The relevant flow velocity v_{GVC} is the same as for the guide vanes, while the hydraulic diameter $d_{h,GVC}$ is calculated with equation (49), already utilized for the annular runner section of the Type 1400 RCP. With the known dimensions and velocities, the dimension factor $\kappa_{d,GVC}$ and the velocity factor $\kappa_{u,GVC}$ can be determined with equation (50) and (48). The friction coefficients λ_{GVC} and $\lambda_{GVC,ref}$ and the specific energy loss due to friction $E_{LF,GVC}$ are also determined with the equations utilized for the runner section, by simply substituting the RUC-values with the GVC-values in equation (51), (52), and (54). The results for the two pumps are shown in Table 20 and 21.

	$\boldsymbol{d_{h,GVC}}$	$\boldsymbol{\kappa_{d,GVC}}$	$\boldsymbol{v_{GVC}}$	$\boldsymbol{\kappa_{u,GVC}}$
	$[m]$	[-]	$[\frac{m}{s}]$	[-]
Type 1134 RCP	0,12164	0,408	7,438	0,329
Type 1400 RCP	0,15519	0,427	7,153	0,376

Table 20: Hydraulic diameter, dimension factor, mean velocity and velocity factor for the annular guide vane channel of the studied RCPs

	$\boldsymbol{\lambda_{GVC}}$	$\boldsymbol{\lambda_{GVC,ref}}$	$\boldsymbol{E_{Lf,GVC}}$
	[-]	[-]	$[\frac{m^2}{s^2}]$
Type 1134 RCP	0,0129	0,0116	0,265
Type 1400 RCP	0,0125	0,0113	0,495

Table 21: Friction coefficients, and specific energy loss due to friction for the annular guide vane section of the studied RCPs

5.4.3 Guide vane section scale-up factors

The scale-up factors for the guide vane section are summarized in Table 22 and 23. The friction factors $C_{f,GVS,ref}$ and $C_{f,GVS}$, the dimension factor $\kappa_{d,GVS}$ and the velocity factor $\kappa_{u,GVS}$ are set equal to the values calculated for the guide vanes, as they cause the majority of the friction losses in the guide vane section. The specific hydraulic energy loss due to friction $E_{Lf,RU}$ of the section is obtained by adding the friction losses of the annular channel to those of the guide vanes, as shown in equation 63. With the friction losses and the dimension, velocity, and friction factors, it is then possible to determine the relative and reference scalable hydraulic energy loss $\delta_{E,GV}$ and $\delta_{E,GV,ref}$, and the scalable hydraulic energy loss index $d_{E,GV,ref}$, by inserting in equation (56), (57), and (58) the values for the guide vane section.

$$E_{Lf,GVS} = E_{Lf,GV} + E_{Lf,GVC} \tag{63}$$

	$\boldsymbol{\kappa_{d,GVS}}$	$\boldsymbol{\kappa_{u,GVS}}$	$\boldsymbol{E_{Lf,GVS}}$
	[-]	[-]	$[\frac{m^2}{s^2}]$
Type 1134 RCP	0,30225	0,32901	5,231
Type 1400 RCP	0,66324	0,37586	5,494

Table 22: Dimension factor, velocity factor, and specific energy loss due to friction for the guide vane section of the studied RCPs

	$\boldsymbol{\delta_{E,GV}}$	$\boldsymbol{\delta_{E,GV,ref}}$	$\boldsymbol{d_{E,GV,ref}}$
	[-]	[-]	[-]
Type 1134 RCP	0,0401	0,0382	0,0330
Type 1400 RCP	0,0366	0,0352	0,0296

Table 23: Relative and reference scalable hydraulic energy loss, and scalable hydraulic energy loss index for the guide vane section of the studied RCPs

5.5 Scale-up factors for the cylindrical casing

The cylindrical RCP casing shown in Figure 13, has an annular inlet and the outlet-pipe connected to the cylindrical wall. Due to the complex flow dynamics in the casing, the friction losses can't be accurately approximated by known formulas for pipes or flat plates. For this reason, a CFD-analysis of the casing-flow was carried out. The analysis provided the average flow velocity v_{CY} inside the component, necessary to compute the velocity factor $\kappa_{u,CY}$, and, by integrating the wall shear stress over the surface of the casing, the friction force $F_{f,CY}$ on the walls was obtained. As shown in Section 5.5.3, it is then possible to calculate the remaining scale-up factors of the component, with the data provided by the analysis.

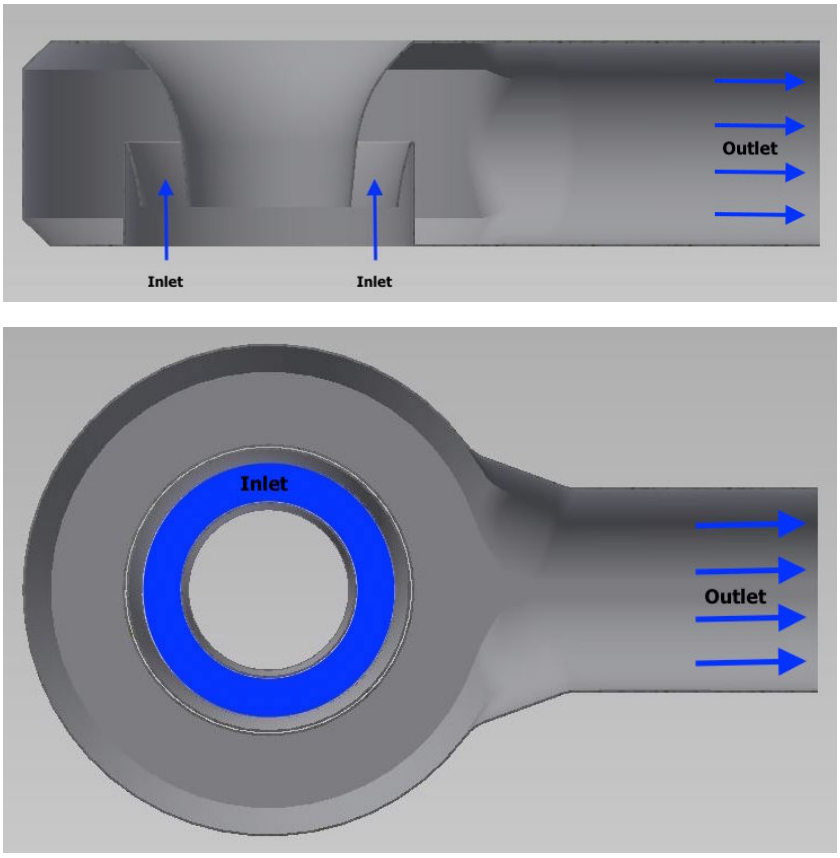

Figure 13: Cylindrical RCP casing, vertical and horizontal section view

5.5.1 CFD-analysis

The CFD-analysis of the cylindrical casing was realized with the commercial software *ANSYS Fluent*, while the model-mesh was generated with the software *ANSYS ICEM*. The first step was to draw a 3D-model of the water volume inside the two investigated casings, by using the CAD-program *Autodesk Inventor*, and to lower the computation time of the CFD-simulation, only the symmetric half of the water volume was modeled. The geometric data of the reactor coolant pumps were provided by *ANDRITZ AG* in the form of technical drawings. The 3D-model was then loaded into the meshing program *ANSYS ICEM* and meshed with hexahedron blocks, as shown in Figure 14.

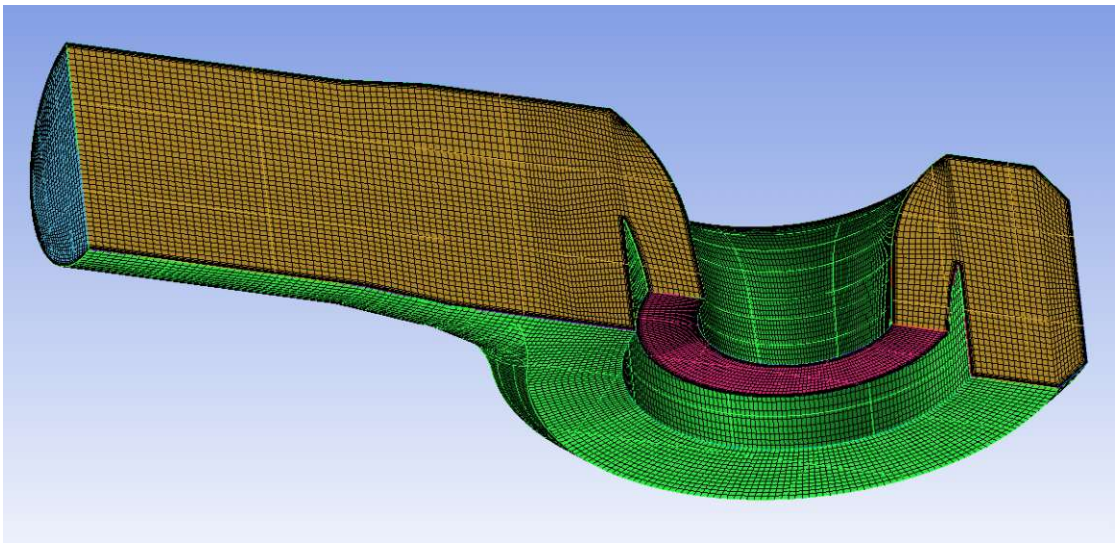

Figure 14: Meshed model of the Type 1134 RCP casing

Table 24 summarizes the mesh parameters and quality characteristics, by indicating the element angles and 3x3x3 determinants. As shown in the table, the element angles of both RCPs are above 18°, while the 3x3x3 determinants are above 0,3. It is also to note, that the mesh was refined close to the casing walls, to allow the accurate simulation of the flow effects near the walls. With the near-wall

refinement, the y^+ values of the Type 1134 casing reached a maximum of 3,25 and the y^+ values of the Type 1400 casing a maximum of 5,00. y^+ values ≤ 5 result in more accurate results when simulating with the SST $k-\omega$ solution method, as it utilizes near-wall modeling, which works best with y^+ values inside the viscous sublayer [9].

		Type 1134 RCP	Type 1400 RCP
Hexa cell number	[-]	581530	517516
Grid volume	$[m^3]$	0,042934	0,067658
Representative cell size	$[m]$	0,00420	0,00508
3x3x3 Determinants	[-]	$> 0{,}3$	$> 0{,}3$
Element angles	[°]	> 18	> 18

Table 24: Mesh parameters of the simulated RCP casing models

As mentioned above, for the simulation in ANSYS Fluent, the SST $k-\omega$ turbulence model was used. It is a two-equation eddy-viscosity model, in which the Shear Stress Transport (SST) formulation combines the advantages of the $k-\epsilon$ and the $k-\omega$ model. The inner parts of the boundary layer, including the viscous sublayer, are simulated with the $k-\omega$ formulation, while in the free stream the model switches to a $k-\epsilon$ behavior. In this way, the problem of the $k-\omega$ model, of being too sensitive to the inlet free-stream turbulence properties, and that of the $k-\epsilon$ model, of being too stiff when the equations are integrated through the viscous sublayer, is avoided [3].

The model boundaries were chosen so that the casing inlet matches the outlet of the guide vanes and the casing outlet ends at 300mm of the outlet pipe. In this way, the approximated assumption of an inlet and outlet flow perpendicular to the inlet/outlet area as boundary condition can be made. Table 25 indicates the

input boundary conditions for the two models at the optimum efficiency point and constant rotational speed (1450 rpm for the Type 1134 RCP and 1000 rpm for the Type 1400 RCP). At the inlet, the mass flow and an initial gauge pressure are set as boundary conditions, while at the outlet the outlet gauge pressure is used. The pressures set as boundary conditions were obtained through pressure measurements, carried out by *ANDRITZ AG* at different positions in the pump casing [1].

		Type 1134 RCP	Type 1400 RCP
Inlet mass flow	$[\frac{kg}{s}]$	121,516	198,841
Inlet initial gauge pressure	$[Pa]$	297789	273495
Inlet turbulence intensity	[%]	0,05	0,05
Outlet gauge pressure	$[Pa]$	287548	263495
Outlet turbulence intensity	[%]	0,05	0,05
Wall shear condition	[-]	No slip	No slip
Wall sand grain roughness	$[m]$	0,00001	0,00001

Table 25: Boundary conditions of the simulated RCP casing models

The simulation of the best efficiency points, specified in Table 1, was carried out at steady-state conditions, with the solution methods indicated in Table 26. The iteration maximum was set to 3000 for the Type 1134 RCP casing and to 2000 for the Type 1400 RCP casing. Figure 15 and 16 show the streamlines with a velocity magnitude coloration and the wall shear stress for the simulated Type 1134 RCP casing. The resulted average flow velocity in the casing and the wall shear force, obtained by integrating the shear stress over the casing surface, are indicated in Table 27. When the results were computed, the modeled 300mm long outlet pipe was omitted since the scale-up factors should represent only the cylindrical casing, as shown in Figure 16.

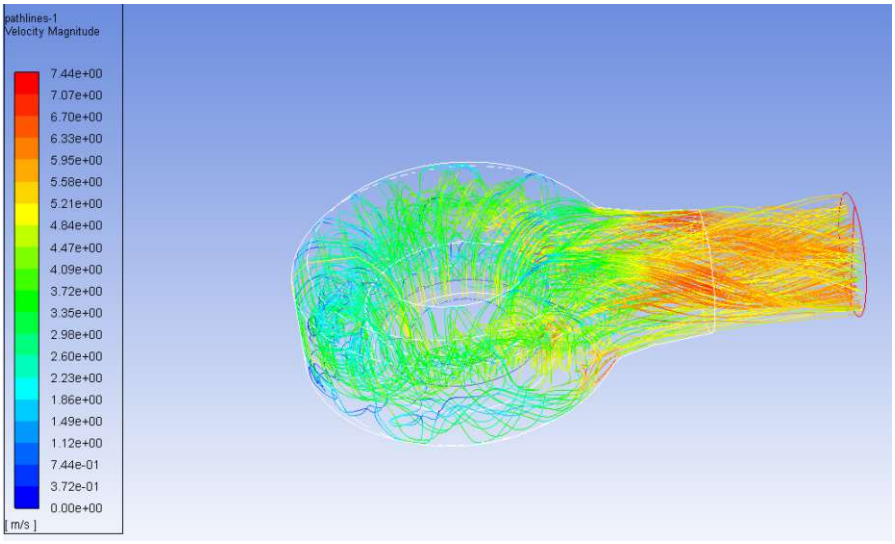

Figure 15: Streamlines and velocities inside the Type 1134 RCP casing

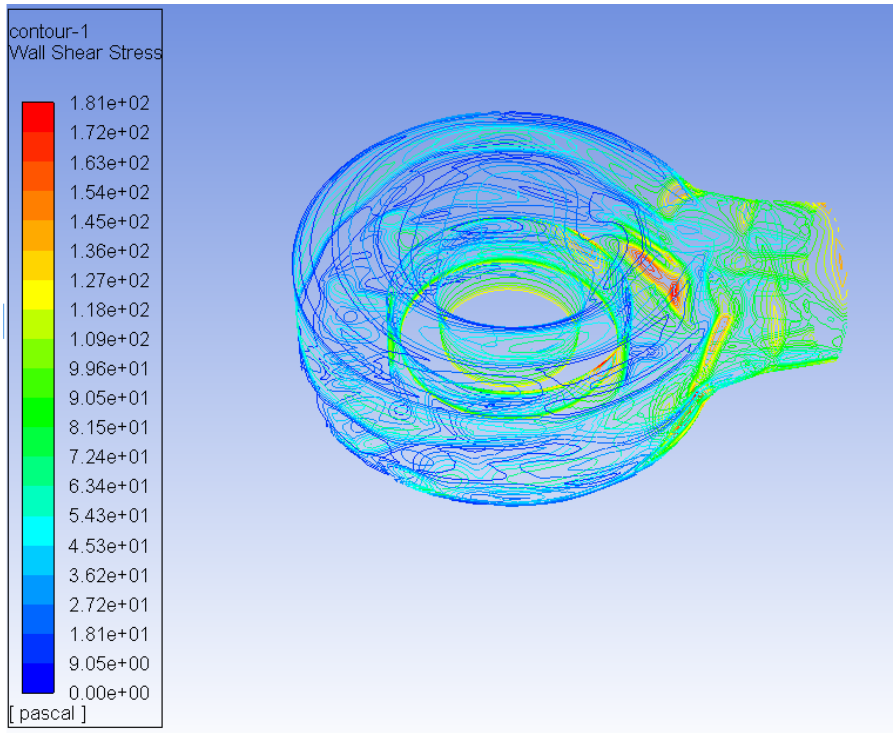

Figure 16: Wall shear stress on the Type 1134 RCP casing surface

	Type 1134 RCP	Type 1400 RCP
Solver	Pressure-based	Pressure-based
Scheme	SIMPLE	SIMPLE
Spacial discretization gradient	Least Squares Cell Based	Least Squares Cell Based
Spacial discretization pressure	Second Order	Second Order
Spacial discretization momentum	Second Order Upwind	Second Order Upwind
Spacial discretization turbulent kinetic energy	Second Order Upwind	Second Order Upwind
Spacial discretization specific dissipation rate	Second Order Upwind	Second Order Upwind

Table 26: *ANSYS Fluent* solution methods of the RCP casing models

		Type 1134 RCP	Type 1400 RCP
Average velocity in the casing	$[\frac{m}{s}]$	3,707	3,597
Wall shear force	$[N]$	56,042	70,464

Table 27: Average velocity and wall shear force of the RCP casing models

5.5.2 Grid independence study

To ensure that the simulated model-meshes converge asymptotically towards the exact solution when refining the meshes, a grid independence study was conducted. The utilized Richardson- Extrapolation requires three distinct meshes (coarse, medium and fine), which were studied, to ensure that the asymptotic range is achieved. Index 1 refers to the fine grid, index 2 to the medium (reference) grid and index 3 to the coarse grid. The procedure follows the ASME guideline for estimation and reporting of uncertainty in CFD applications [2]. The observed parameter is the head difference ΔH between casing inlet and outlet, determined through the total pressure difference of the three simulated grids. As suggested by the guideline, a refinement factor r greater than 1,3 is chosen and indicated in Table 28 for each RCP. The refinement factor r is equal to the ratio of the representative cell height h of two grids, which can be determined through equation (64) and is shown, with the other grid parameters, in Table 24.

$$h = \left(\frac{V}{N}\right)^{1/3} \tag{64}$$

with N = total number of cells and V = grid volume

	medium-fine grid	coarse-medium grid
	$\boldsymbol{r}_{21}$	$\boldsymbol{r}_{32}$
Type 1134 RCP	1,331	1,360
Type 1400 RCP	1,346	1,385

Table 28: Refinement factors of the investigated model grids

With the known refinement factors r_{21} and r_{32}, the extrapolated values $\phi_{ext,21}$ and $\phi_{32,ext}$ can be determined with equation (65). ϕ stands for the observed parameter

and p for the apparent order of the method, obtained through iteration with the procedure presented in reference [2]. At this point, the approximate relative errors e_a and the extrapolated relative errors e_{ext} can be calculated with equation (66) and (67). The grid convergence indexes GCI result from equation (68) and are shown in Table 29, with the other just described values. The asymptotic range is reached if equation (69) is fulfilled [11]. As the refinement factors for the medium-fine grid r_{21} and coarse-medium grid r_{32} differ just marginally, the average value r is used in the equation. The results are presented in the last row of Table 29 and show that the asymptotic range is achieved for the grids of both models (values $\simeq 1$). Figure 17 and 18 validate the results, as the asymptotic character of the convergence curve is clearly visible.

$$\phi_{ext,21} = \frac{r_{21}^p \cdot \phi_1 - \phi_2}{r_{21}^p - 1} \tag{65}$$

$$e_{a,21} = \left| \frac{\phi_1 - \phi_2}{\phi_1} \right| \tag{66}$$

$$e_{ext,21} = \left| \frac{\phi_{ext,21} - \phi_1}{\phi_{ext,21}} \right| \tag{67}$$

$$GCI_{21} = \frac{1,25 \cdot e_{a,21}}{r_{21}^p - 1} \tag{68}$$

$$\frac{r^p \cdot GCI_{21}}{GCI_{32}} \simeq 1 \tag{69}$$

		Type 1134 RCP	**Type 1400 RCP**
Apparent order	p	4,015	5,411
Extrapolated value $[m]$ (medium-fine grid)	$\Delta H_{ext,21}$	1,389	0,804
Extrapolated value $[m]$ (coarse-medium grid)	$\Delta H_{ext,32}$	1,389	0,804
Approximate relative error [%] (medium-fine grid)	$e_{a,21}$	6,919	1,642
Approximate relative error [%] (coarse-medium grid)	$e_{a,32}$	26,547	10,062
Extrapolated relative error [%] (medium-fine grid)	$e_{ext,21}$	3,110	0,411
Extrapolated relative error [%] (coarse-medium grid)	$e_{ext,32}$	9,814	2,046
Grid convergence index (medium-fine grid)	GCI_{21}	4,013	0,515
Grid convergence index (coarse-medium grid)	GCI_{32}	13,602	2,611
Asymptotic range requirement (value $\simeq 1$)	$\frac{r^p \cdot GCI_{21}}{GCI_{32}}$	0,971	1,064

Table 29: Results of the grid independence study

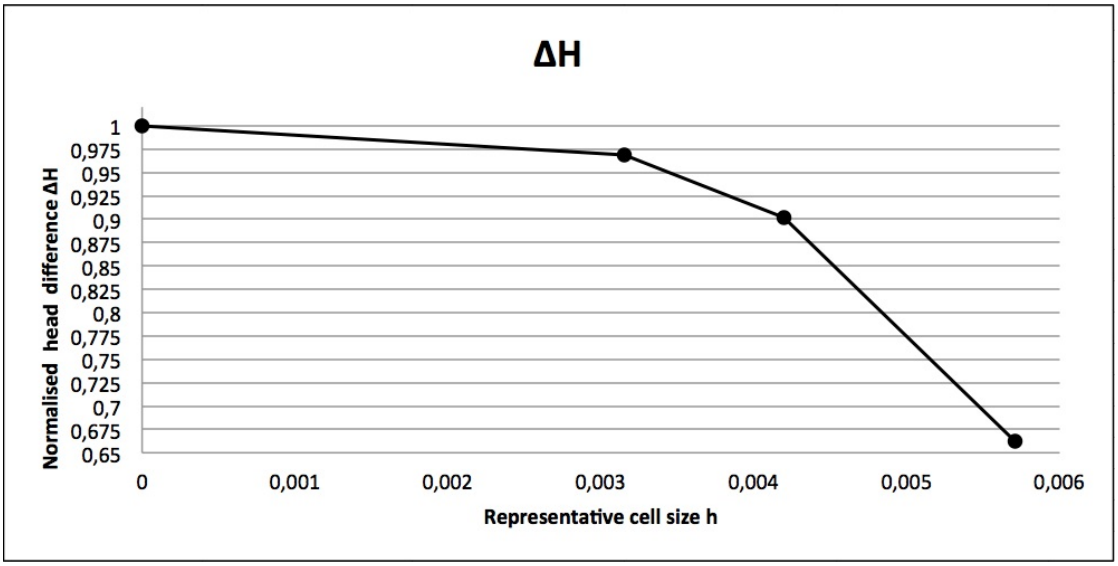

Figure 17: Asymptotic convergence of the head difference for the Type 1134 RCP

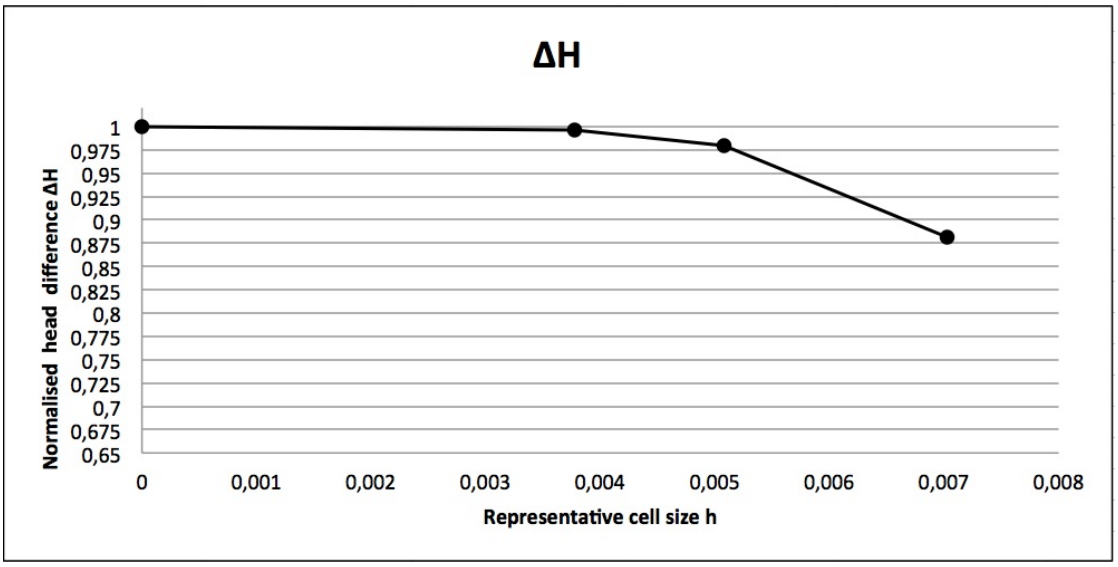

Figure 18: Asymptotic convergence of the head difference for the Type 1400 RCP

5.5.3 Cylindrical casing scale-up factors

With the average flow velocity in the casing v_{CY} and the wall shear force $F_{f,CY}$ (Table 27), obtained through the simulation, it is now possible to determine the scale-up factors for the cylindrical casing. The dimension factor $\kappa_{d,CY}$ is defined as the ratio of the hydraulic diameter of the casing $d_{h,CY}$ to the reference pump diameter. Due to the complex geometry, the hydraulic diameter is approximated by averaging the hydraulic diameters of the annular casing inlet section, the cylindrical casing section, and the outlet section. The individual hydraulic diameters were determined through equation (49), and the average value is presented with the resulted dimension factor $\kappa_{d,CY}$ in Table 30. The table also shows the velocity factor $\kappa_{u,CY}$, which is determined by inserting the average flow velocity v_{CY}, obtained from the simulation, in equation (21). Equation (71) provides the specific energy loss due to friction $E_{Lf,CY}$. In the equation, the wall shear force $F_{f,CY}$ is divided by the density ρ_W and the sectional area of the flow A_{CY}, obtained by averaging the sectional areas utilized to determine the mean hydraulic diameter. The equation is derived from equation (70), which sets the friction force generated on the channel walls equal to the pressure drop Δp multiplied by the cross-sectional area of the flow and equal to the shear stress integrated over the channel surface [10].

$$F_f = \Delta p \cdot A_{channel} = \iint_S \tau_{wall} dS_{wall} \quad \text{with} \quad \frac{\Delta p}{\rho_W} = E_{Lf} \tag{70}$$

with $A_{channel}$ = cross-sectional area of the flow & S_{wall} = channel wall surface

$$E_{Lf,CY} = \frac{F_{f,CY}}{A_{CY} \cdot \rho_W} \tag{71}$$

	$d_{h,CY}$	$\kappa_{d,CY}$	$\kappa_{u,CY}$	$E_{Lf,CY}$
	[m]	[-]	[-]	$[\frac{m^2}{s^2}]$
Type 1134 RCP	0,20609	0,69210	0,16396	0,928
Type 1400 RCP	0,24591	0,67655	0,18899	0,772

Table 30: Dimension factor, velocity factor, and specific energy loss due to friction for the cylindrical casing of the studied RCPs

The energy loss due to friction $E_{Lf,CY}$ is then divided by the specific energy $E_{h,M}$ of the pump in equation (72), to obtain the relative scalable hydraulic energy loss $\delta_{E,CY}$. As for the other components, the reference scalable hydraulic energy loss can be calculated by multiplying $\delta_{E,CY}$ by the ratio of the reference friction factor $\lambda_{CY,ref}$ to the regular friction factor λ_{CY}. The friction factors in equation (73) are obtained from equation (51) and (52), by substituting the values of the runner channel with those of the cylindrical casings. The scalable hydraulic energy loss index $d_{E,CY,ref}$ can then be determined through equation (74), from the previously calculated factors [4].

$$\delta_{E,CY} = \frac{E_{Lf,CY}}{E_{h,M}} \tag{72}$$

$$\delta_{E,CY,ref} = \frac{\lambda_{CY,ref}}{\lambda_{CY}} \tag{73}$$

$$d_{E,CY,ref} = \frac{\delta_{E,CY,ref}}{1 + 0.351 \cdot (\kappa_{u,CY} \cdot \kappa_{d,CY})^{0.2}} \tag{74}$$

	λ_{CY}	$\lambda_{CY,ref}$	$\delta_{E,CY}$	$\delta_{E,CY,ref}$	$d_{E,CY,ref}$
	[-]	[-]	[-]	[-]	[-]
Type 1134 RCP	0,0127	0,0119	0,00712	0,00667	0,00544
Type 1400 RCP	0,0124	0,0117	0,00515	0,00486	0,00394

Table 31: Friction factors, relative and reference scalable hydraulic energy loss, and scalable hydraulic energy loss index for the cylindrical casing of the studied RCPs

5.6 Scale-up factors for shroud ring friction

As mentioned in chapter 5.1, only the Type 1400 RCP has a shroud ring connected to the blade tips, which generates friction losses affecting the mechanical power P_m. Hence, the losses affecting the mechanical power of the Type 1134 RCP are considered negligible, as the area of the blade tips is much smaller than the external shroud ring surface of the Type 1400 RCP.

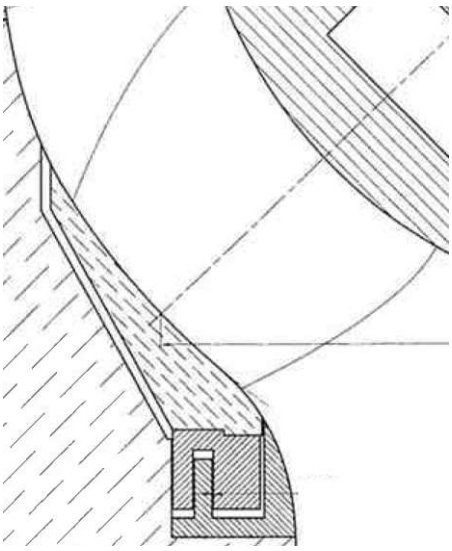

Figure 19: Shroud ring connected to one of the Type 1400 RCP runner blades [1]

The losses caused by the friction of the flow between the external surface of the shroud ring and the casing are calculated with the equations describing the flow between two rotating cylinders. The friction loss coefficient $C_{T,SR}$ is obtained through equation (76), with the rotational Reynolds number $R\omega$ defined in equation (75) [8]. By inserting the friction coefficient $C_{T,SR}$ in equation (77), it is then possible to determine the power loss $P_{Lf,SR}$ due to shroud ring friction. Equation (78) defines the relative scalable friction loss δ_T, as the ratio of the power loss $P_{Lf,SR}$ to the mechanical power $P_{m,M}$ of the pump. To obtain the reference value $\delta_{T,ref}$ with equation (80), it is first necessary to calculate the friction coefficient at reference condition $C_{T,SR,ref}$, by inserting the reference rotational speed ω_{ref} (equation (79)) in equation (75) and (76). As the wall-roughness is not considered in the friction factor, the scalable friction loss index d_T coincides with the reference scalable friction loss δ_T. The friction factors and the rotational Reynolds numbers of the Type 1400 pump are indicated in Table 32, while the mechanical power loss, the relative and reference scalable friction loss, and the scalable friction loss index are presented in Table 33.

$$R\omega = \frac{r_{SR} \cdot \omega \cdot b}{\nu_W} \tag{75}$$

with $r_{SR} = \frac{D_{SR}}{2}$; $\omega = 2 \cdot \pi \cdot n$; b =average clearance between cylinders

$$C_{T,SR} = 0,00759 \cdot R\omega^{-0,24} \tag{76}$$

	r_{SR}	$R\omega$	$R\omega_{ref}$	$C_{T,SR}$	$C_{T,SR,ref}$
	[m]	[-]	[-]	[-]	[-]
Type 1400 RCP	0,1986	67654	68707	0,00053	0,00052

Table 32: Shroud ring radius, rotational Reynolds numbers, and friction coefficients for the shroud ring of the Type 1400 RCP

$$P_{Lf,SR} = C_{T,SR} \cdot 2 \cdot \pi \cdot \rho_W \cdot \omega^3 \cdot r_{SR}^4 \cdot L_{SR} \tag{77}$$

with L_{SR} =length of the shroud ring

$$\delta_T = \frac{P_{Lf,SR}}{P_{m,M}} \tag{78}$$

$$\omega_{ref} = \frac{2 \cdot \nu_W \cdot Re_{ref}}{D_M^2} \tag{79}$$

$$\delta_{T,ref} = \frac{C_{T,SR,ref}}{C_{T,SR}} \cdot \delta_T \tag{80}$$

	$\boldsymbol{P}_{Lf,SR}$	$\boldsymbol{\delta}_{T,SR}$	$\boldsymbol{\delta}_{T,SR,ref}$	$\boldsymbol{d}_{T,SR,ref}$
	$[W]$	[-]	[-]	[-]
Type 1400 RCP	619,077	0,00856	0,00852	0,00852

Table 33: Mechanical power loss due to friction, relative and reference scalable hydraulic energy loss, and scalable hydraulic energy loss index of the Type 1400 RCP shroud ring

6 Summary of the results

The factors determined in chapter 5 for each component, and necessary to scale-up the performance of RCP models, are summarized in Table 34, 35, 36, and 37. These factors will be linearly interpolated in section 6.1, to obtain linear functions depending upon the specific speed N_{QE} of the machine to be scaled-up. With the linear functions, it is then possible to scale-up RCPs by applying the formulas in chapter 7, which were derived from the IEC 62097 standard.

RUNNER SCALE-UP FACTORS			
	Velocity factor $\boldsymbol{\kappa_u}$	Reference scalable energy loss $\boldsymbol{\delta_{E,ref}}$	Scalable energy loss index $\boldsymbol{d_{E,ref}}$
Type 1134 RCP	0,6311	0,0408	0,0336
Type 1400 RCP	0,6482	0,0371	0,0308

Table 34: Scale-up factors for the runner of the studied RCPs

GUIDE VANE SECTION SCALE-UP FACTORS			
	Velocity factor $\boldsymbol{\kappa_u}$	Reference scalable energy loss $\boldsymbol{\delta_{E,ref}}$	Scalable energy loss index $\boldsymbol{d_{E,ref}}$
Type 1134 RCP	0,3290	0,0382	0,0330
Type 1400 RCP	0,3759	0,0352	0,0296

Table 35: Scale-up factors for the guide vane section of the studied RCPs

CYLINDRICAL CASING SCALE-UP FACTORS			
	Velocity factor $\boldsymbol{\kappa}_u$	Reference scalable energy loss $\boldsymbol{\delta}_{E,ref}$	Scalable energy loss index $\boldsymbol{d}_{E,ref}$
Type 1134 RCP	0,1640	0,00667	0,00544
Type 1400 RCP	0,1890	0,00486	0,00394

Table 36: Scale-up factors for the cylindrical casing of the studied RCPs

SHROUD RING SCALE-UP FACTORS		
	Reference scalable energy loss $\boldsymbol{\delta}_{T,ref}$	Scalable energy loss index $\boldsymbol{d}_{T,ref}$
Type 1400 RCP	0,00852	0,00852

Table 37: Scale-up factors for the shroud ring of the Type 1400 RCP

6.1 Derived linear functions for scale-up factors

The scale-up factors for each component can now be transposed into linear functions, by plotting the values according to the specific speed N_{QE} of each studied RCP and then linearly interpolate the plotted points. The specific speed N_{QE} of the RCPs is obtained from equation (81) [4] and presented in Table 38. With the known specific speed, it is then possible to plot all the factors and obtain a linear function for each component. The plots and the resulted functions are shown in Figure 20, 21, and 22.

$$N_{QE} = \frac{n_{M,opt} \cdot Q_{M,opt}^{0,5}}{E_{M,opt}^{0,75}} \tag{81}$$

	Type 1134 RCP	Type 1400 RCP
Specific speed N_{QE}	0,30908	0,24549

Table 38: Specific speed of the studied RCPs

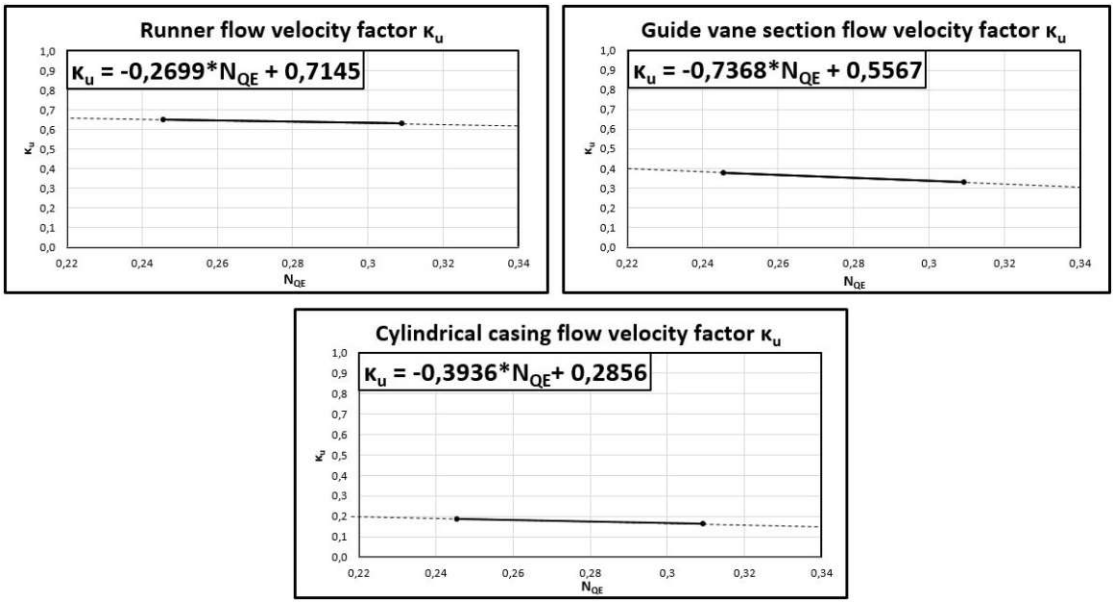

Figure 20: Flow velocity factor of each component

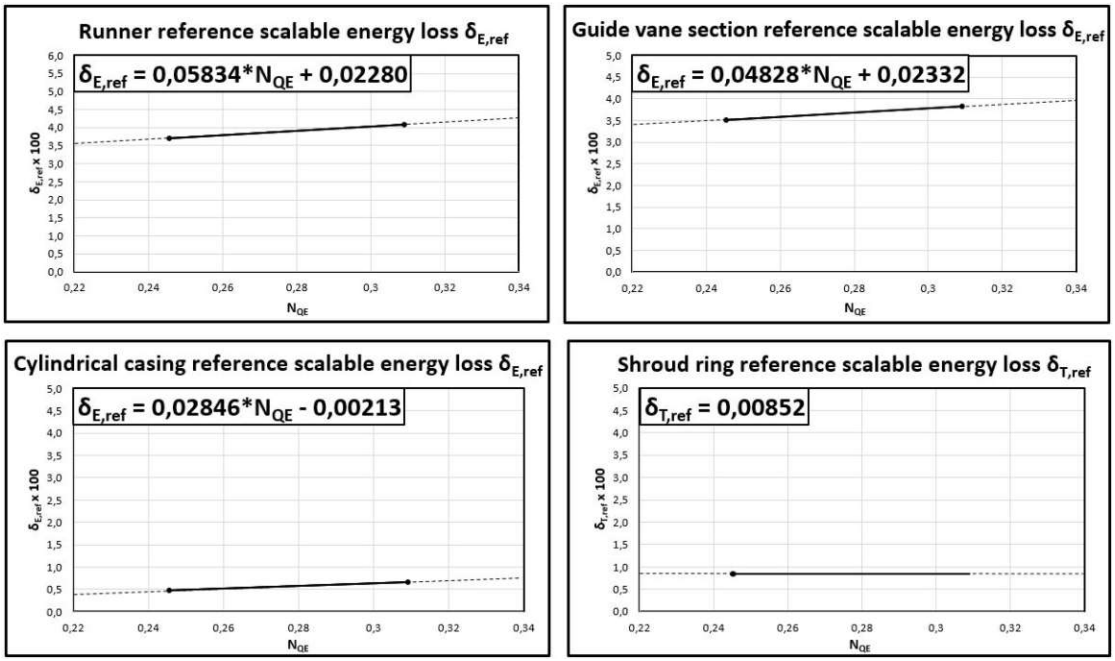

Figure 21: Reference scalable energy loss of each component

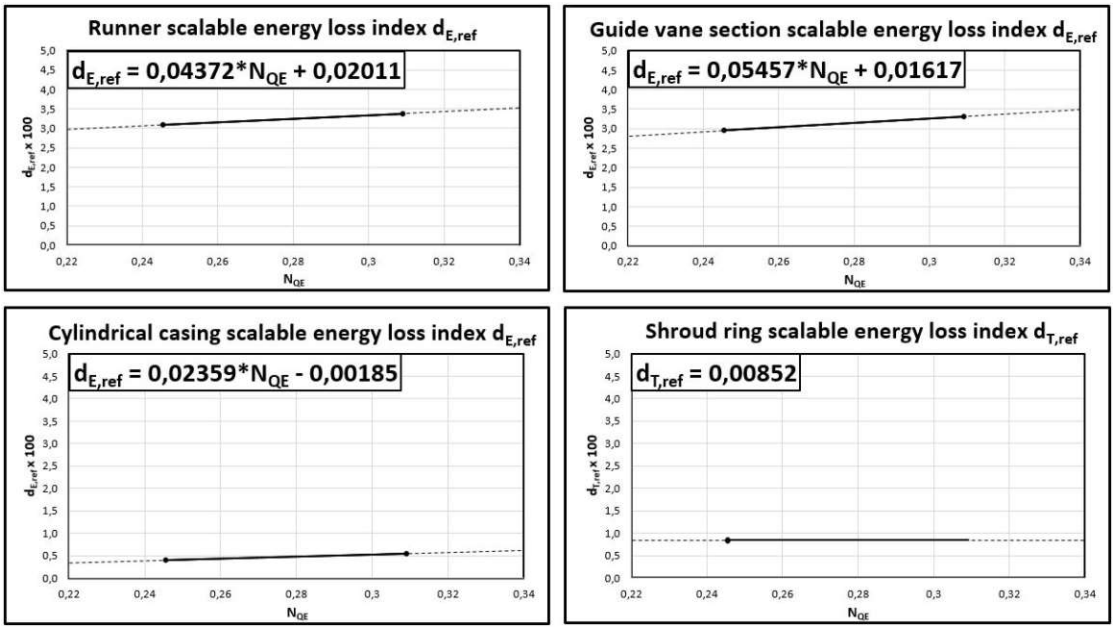

Figure 22: Scalable energy loss index of each component

6.2 Flux diagrams

The flux diagrams below show how the losses affect the efficiency of the two RCPs. The shroud ring losses reduce the mechanical input energy of the pump, while the losses of the runner, guide vane section, and cylindrical casing affect the specific hydraulic energy. The diagrams also indicate the amount of scalable (friction) losses and non-scalable (kinetic) losses for each component. While for the runner roughly 50% of the runner losses are scalable and for the guide vane section 60% are scalable, the loss subdivision for the cylindrical casing is considerably less balanced, since only roughly 10% of the casing losses are considered scalable. The source of this unbalance is the cylindrical casing shape, which generates unfavorable flow dynamics inside the casing, but is necessary for safety reasons, as the cylindrical shape allows for reliable X-ray testing during production.

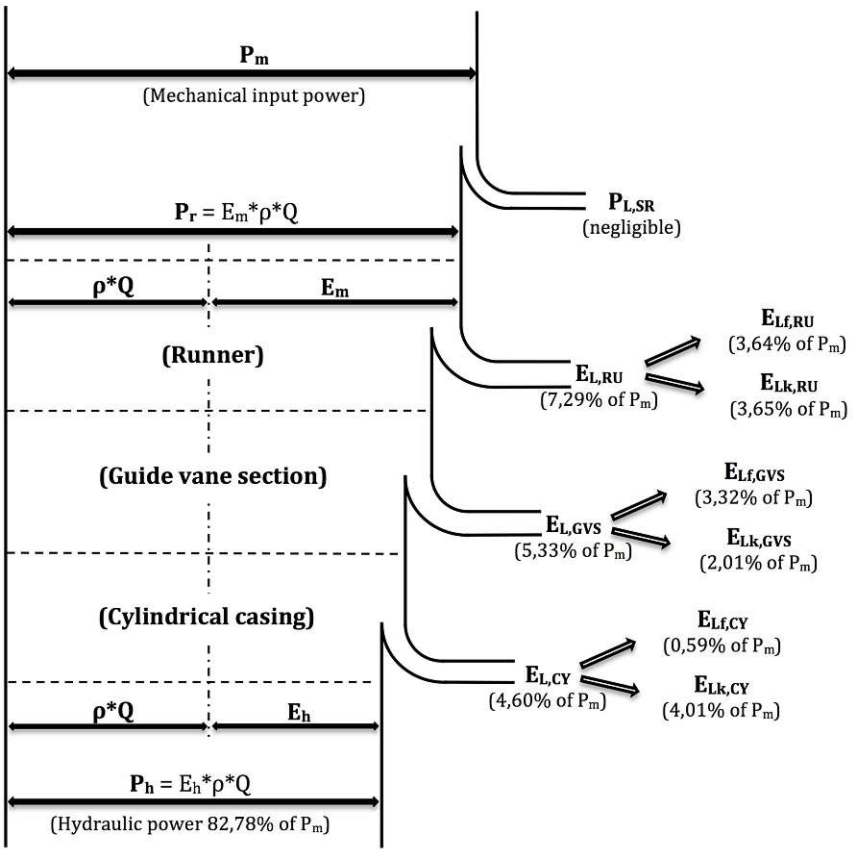

Figure 23: Flux diagram for the Type 1134 RCP

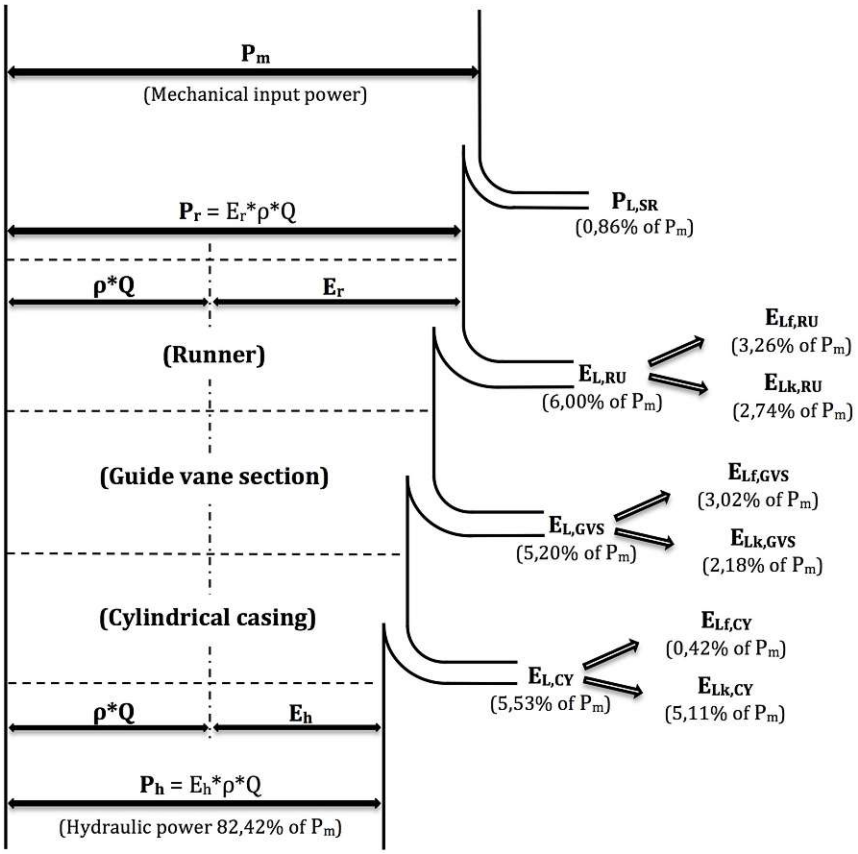

Figure 24: Flux diagram for the Type 1400 RCP

7 Model to prototype performance scale-up

The procedure to scale up the model performance data to the prototype, according to IEC 62097, was presented in chapter 4.2. The component subdivision in the standard is slightly different than the one performed for the investigated RCPs and for that reason, the formulas to calculate the efficiency step-up ratio Δ of each component are presented once more below. Equation (82) applies to the runner and the guide vane section, equation (83) to the cylindrical casing, and equation (84) to the shroud ring of the Type 1400 RCP. The equations are obtained by entering the friction coefficients of each component into the definition of the efficiency step-up ratio in equation (85), (86), and (87) [4]. With the pump data and the equations for the scale-up factors κ_u and d_{ref} introduced in chapter 6.1, the model performance of RCPs can then be scaled up to the prototype. An example of the performance scale-up calculation for the Type 1400 RCP is presented in section 7.1.

$$\Delta_{E,RU/GVS} = d_{E,CO,ref} \cdot \left[\left(5 \cdot 10^5 \cdot \kappa_{u,CO} \cdot \frac{Ra_{CO,M}}{D_M} + \frac{Re_{ref}}{Re_M} \right)^{0,2} - \left(5 \cdot 10^5 \cdot \kappa_{u,CO} \cdot \frac{Ra_{CO,P}}{D_P} + \frac{Re_{ref}}{Re_P} \right)^{0,2} \right] \tag{82}$$

$$\Delta_{E,CY} = d_{E,CO,ref} \cdot \left[\left(4 \cdot 10^5 \cdot \kappa_{u,CO} \cdot \frac{Ra_{CO,M}}{D_M} + \frac{Re_{ref}}{Re_M} \right)^{0,2} - \left(4 \cdot 10^5 \cdot \kappa_{u,CO} \cdot \frac{Ra_{CO,P}}{D_P} + \frac{Re_{ref}}{Re_P} \right)^{0,2} \right] \tag{83}$$

$$\Delta_{T,SR} = d_{T,ref} \cdot \left[\left(\frac{Re_{ref}}{Re_M} \right)^{0,24} - \left(\frac{D_P}{D_M} \cdot \frac{Re_{ref}}{Re_P} \right)^{0,24} \right] \tag{84}$$

$$\Delta_{E,RU/GVS} = \delta_{E,ref} \cdot \left(\frac{C_{f,M} - C_{f,P}}{C_{f,ref}} \right) \tag{85}$$

$$\Delta_{E,CY} = \delta_{E,ref} \cdot \left(\frac{\lambda_M - \lambda_P}{\lambda_{ref}} \right) \tag{86}$$

$$\Delta_{T,SR} = \delta_{T,ref} \cdot \left(\frac{C_{T,M} - C_{T,P}}{C_{T,ref}} \right) \tag{87}$$

7.1 Example of model-prototype step-up calculation

The following step up calculation is carried out for the Type 1400 RCP at the best efficiency point, indicated in Table 39. The table shows also the wall roughnesses and the necessary input data of model and prototype. The RCP seals are considered to be homologous so that the volumetric efficiency η_Q results equal to 1. Appendix B shows the complete scale-up calculation, performed with the software *Mathcad Prime*.

As a first step, the velocity factors κ_u and the scalable energy loss indexes d_{ref} can be computed for each component, by inserting the specific speed N_{QE} in the equations presented in chapter 6.1. The obtained loss indexes are presented with the velocity factors κ_u in Table 40. Once the scale-up factors are determined, the efficiency step-up ratios Δ can be computed for each component with equation (82), (83), and (84). By making the sum of $\Delta_{E,RU}$, $\Delta_{E,GVS}$, and $\Delta_{E,CY}$, the total efficiency step-up ratio affecting the specific hydraulic energy Δ_E is obtained. Δ_E is indicated in Table 40, together with Δ_T affecting the mechanical power, and Δ_Q affecting the discharge, but equal to 0 since the seals are homologous. By inserting the calculated efficiency step-up ratios in equation (29), (30), (32), and (31), the model performance data can be scaled-up to the prototype. The resulted prototype performance is presented in Table 41 and shows an efficiency increased from model to prototype of 2,03%.

		Model	**Prototype**
Reference diameter	$[m]$	0,363479	0,89
Shaft speed	$[\frac{1}{s}]$	16,65	19,833
Discharge	$[\frac{m^3}{s}]$	0,398	-
Specific hydraulic energy	$[\frac{m^2}{s^2}]$	149,655	-
Mechanical power	$[kW]$	72,171	-
Hydraulic efficiency	[%]	82,4	-
Efficiency at optimum point	[%]	82,5	-
Reference Reynolds number	[-]	$7 \cdot 10^6$	-
Reynolds number	[-]	$6,88583 \cdot 10^6$	$4,07173 \cdot 10^8$
Specific speed	[-]	0,24549	-
Water density	$[\frac{kg}{m^3}]$	998,43	745
Wall roughness of runner	$[\mu m]$	0,5	0,8
Wall roughness of guide vane section	$[\mu m]$	0,5	0,8
Wall roughness of cylindrical casing	$[\mu m]$	2,0	3,2

Table 39: Scale-up input data for the Type 1400 RCP [1]

	Flow velocity factor κ_u	**Scalable hydraulic energy loss index** d_{ref}	**Efficiency step-up ratio** Δ
Runner	0,64824	0,03084	0,00890
Guide vane section	0,37582	0,02957	0,00992
Cylindrical casing	0,18897	0,00394	0,00116
Shroud ring	-	0,00852	0,00457
Total efficiency step-up ratio Δ_E affecting the specific hydraulic energy			0,01998
Total efficiency step-up ratio Δ_T affecting the mechanical power			0,00457
Total efficiency step-up ratio Δ_Q affecting the discharge			0

Table 40: Flow velocity factors, scalable hydraulic energy loss indexes, and efficiency step-up ratios for the Type 1400 RCP

		Prototype
Discharge	$[\frac{m^3}{s}]$	6,9598
Specific hydraulic energy	$[\frac{m^2}{s^2}]$	1298,57
Mechanical power	$[kW]$	7974,82
Hydraulic efficiency	[%]	84,43

Table 41: Prototype performance of the Type 1400 RCP

7.2 Influence of prototype wall-roughness

As mentioned in chapter 4.3, the additional consideration of wall roughness in the scale-up process is one of the main improvements of the IEC 62097 standard over the scale-up procedure presented in the IEC 60193 norm. To examine the influence of different prototype wall roughnesses on the resulted efficiency increase of the scale-up, multiple scale-up calculations, with different wall-roughnesses, have been performed for the two investigated RCPs. From the results presented in Table 99, it is possible to see that, if the surfaces of model and prototype are set as smooth, the efficiency increase reaches its maximum, with 3,69% for the Type 1134 RCP and 3,36% for the Type 1400 RCP, compared to the $\sim$ 2,1% of the regular scale-up. On the other hand, if the wall roughness is gradually increased, the efficiency increase diminishes until reaching 0 or even become negative if the wall roughness is set high enough. This behavior is considered as an improvement since it penalizes hydraulic machines with rougher wall surfaces, which would have the same efficiency increase to machines with smoother walls if scaled-up with the older IEC 60193 procedure.

Type 1134 RCP				**Type 1400 RCP**			
Wall roughness [μm]			$\Delta\eta_{h,M->P}$	Wall roughness [μm]			$\Delta\eta_{h,M->P}$
RU	GVS	CY		RU	GVS	CY	
0,0	0,0	0,0	3,69%	0,0	0,0	0,0	3,36%
0,8	0,8	3,2	2,16% [real values]	0,8	0,8	3,2	2,03% [real values]
2,0	2,0	5,5	1,34%	2,0	2,0	5,5	1,29%
3,0	3,0	8,0	0,90%	3,0	3,0	8,0	0,90%
4,0	4,0	10,5	0,57%	4,0	4,0	10,5	0,60%
5,0	5,0	13,0	0,30%	5,0	5,0	13,0	0,35%
6,0	6,0	15,5	0,07%	6,0	6,0	15,5	0,14%

Table 42: Efficiency difference between model and prototype for different prototype wall roughnesses of the investigated RCPs

7.3 Comparison to IEC 60193 scale-up method

In chapter 4.3 it was mentioned that the scale-up method presented by the IEC 60193 standard overestimates the efficiency increase due to multiple inaccuracies. This fact can be observed by comparing the results of the efficiency scale-up of the investigated RCPs, calculated with the two different methods. The results are presented in Table 43 and it is noticeable that the efficiency difference, obtained through the IEC 60193 procedure, is considerably higher than the one obtained by applying the IEC 62097 standard.

	$\Delta\eta_{h,M->P}$ (IEC 62097)	$\Delta\eta_{h,M->P}$ (IEC 60193)
Type 1134 RCP	2,16%	5,44%
Type 1400 RCP	2,03%	5,05%

Table 43: Efficiency difference between model and prototype for different scale-up methods

The reason behind this difference, other than the general overestimation of the IEC 60193 method, is the fact, that the IEC 62097 procedure includes the effects of the wall roughness difference between model and prototype. This effect can reduce the efficiency, obtained by considering smooth walls, up to 1,5%, as is shown in Table 42, where the IEC 62097 method was applied for smooth and rough wall surfaces. Furthermore, as the IEC 62097 procedure considers each component individually, and just 10% of the cylindrical casings losses are considered scalable, the total amount of scalable losses of RCPs with this type of casing is smaller than for pumps with more favorable casing designs. As already mentioned, the reason for utilizing a cylindrical casing design for reactor coolant pumps lies in the very demanding safety requirements for nuclear power plant equipment. The cylindrical casing shape, being relatively simple, results very suitable for X-ray testing, which is necessary to find unwanted inclusions, cracks or production defects. This casing shape is therefore preferred to more intricate designs (as spiral casings), which are more efficient, but at the same time more difficult to test for faults.

8 Conclusion

The aim of this work was to determine the scale-up factors necessary to apply the IEC 62097 standard to reactor coolant pumps. This was achieved, by studying two RCPs with different specific speeds at the optimum efficiency point. The RCPs were divided into main components, and the scalable losses determined for each of them. For the runner and guide vane section, the friction losses were determined through formulas for friction losses in channel flows and flows over flat plates, provided by the IEC 62097 standard. The friction losses in the cylindrical casing had to be determined through a CFD-analysis of the casing, as the complex casing flow dynamics can't be accurately approximated by common friction loss formulas. The analysis was performed with the commercial software *ANSYS Fluent* and, as a solver, the SST $k-\omega$ solution method was utilized. To ensure the convergence of the grid, a grid independence study was conducted. The Type 1400 RCP was additionally provided with a shroud ring, connected to the runner blade tips, and the losses caused by it were determined via a formula for concentric rotating cylinders.

The flux diagrams in chapter 6.2 show how, for the runner, 50% of its total losses are scalable, for the guide vane section, 60% are scalable, while for the cylindrical casing only 10% of its total losses are considered scalable. This unbalance in the casing losses derives from the cylindrical shape, which is chosen as it allows reliable X-ray testing during production, but doesn't generate convenient flow dynamics.

With the scalable losses, velocities, and geometry of the RCPs, the scale-up factors could be determined for each component and plotted according to the specific speed of the machine. From the plots, linear functions were derived for each component, so that now, once the specific speed of an axial flow RCP at a specific operating point is known, the scale-up factors for that RCP can be easily obtained.

The scale-up method of the IEC 62097 and IEC 60193 standard were compared, by performing scale-up calculations for the investigated RCPs, with both procedures. The results showed the expected overestimation of the efficiency increase from

model to prototype by the IEC 60193 procedure, with an efficiency difference of roughly 5% compared to the 2,1% of the IEC 62097 procedure. To further investigate the differences between the methods, the effects of wall roughness were analyzed in the IEC 62097 procedure and showed that for the studied RCPs, the efficiency difference is reduced up to 1,5%, compared to the scale-up performed with smooth walls. By increasing the roughness of the prototype walls, it was additionally observed that the efficiency difference between model and prototype decreases gradually, which is the desired behavior, as prototypes with rougher surfaces should have a worse efficiency than prototypes with smooth surfaces. This effect is not covered by the IEC 60193 procedure, as it assumes smooth surfaces for the scale-up.

Through the study of the two axial flow RCPs, this work set the groundwork to apply the IEC 62097 standard to this type of pumps. The accuracy of the linear functions, describing the scale-up factors, could be further improved by studying multiple additional axial flow RCPs, with different specific speeds at the optimum efficiency point. By doing so, a greater range of specific speeds could be covered and the linear functions improved, by interpolating more points for each factor.

Appendix A

Computation of scale-up factors for the Type 1134 RCP

(Explanation notes marked in grey)

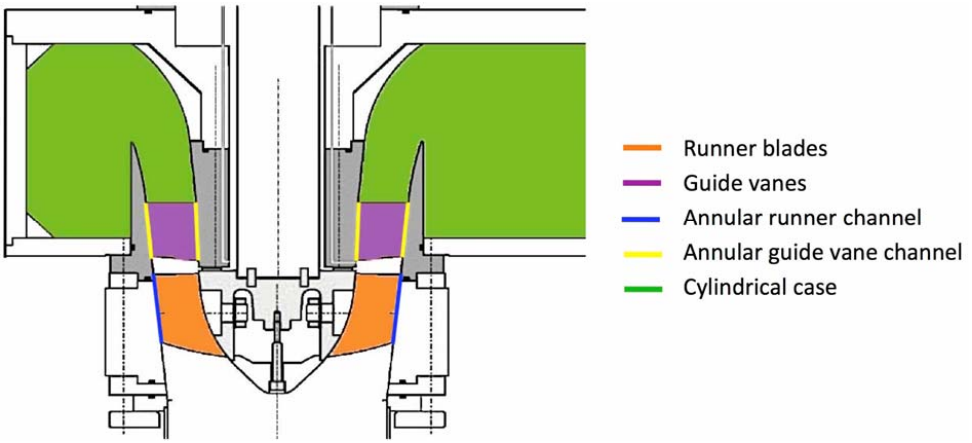

1. Model constant data

Reference diameter:	$D_M := 0.29777\ m$
Local acceleration due to gravity:	$g := 9.80703\ \frac{m}{s^2}$
Reference Reynolds number acc. to IEC:	$Re_{ref} := 7 \cdot 10^6$
Area of high pressure section:	$A_1 := 0.046434\ m^2$
Area of low pressure section:	$A_2 := 0.059115\ m^2$
Zeta of high pressure side:	$\zeta_1 := 0.037$
Zeta of low pressure side:	$\zeta_2 := 0.248$
Wall roughness of runner blades:	$Ra_{RB} := 0.5 \cdot 10^{-6}\ m$
Wall roughness of guide vanes:	$Ra_{GV} := 0.5 \cdot 10^{-6}\ m$
Wall roughness of annular runner channel:	$Ra_{RUC} := 0.8 \cdot 10^{-6}\ m$
Wall roughness of annular guide vane channel:	$Ra_{GVC} := 2 \cdot 10^{-6}\ m$
Wall roughness of cylindrical casing:	$Ra_{CY} := 2 \cdot 10^{-6}\ m$

2. Test point data

Water temperature: $t_W := 17.56\ °C$

Test absolute ambient pressure: $p_{amb.} := 97200\ Pa$

Test point shaft speed: $n_{TP} := \frac{1248.4}{60}\ \frac{1}{s} = 20.80667\ \frac{1}{s}$

Pressure at low pressure section: $p_2 := 101050\ Pa$

Differential pressure high & low pressure section: $p_{12} := 90674\ Pa$

Pressure at high pressure section: $p_1 := p_2 + p_{12} = \left(1.91724 \cdot 10^5\right)\ Pa$

Density of water at high pressure section: $\rho_1 := 998.764\ \frac{kg}{m^3}$

Density of water at low pressure section: $\rho_2 := 998.722\ \frac{kg}{m^3}$

Discharge calculation from Venturi tube measurements

Differential pressure at Venturi nozzle: $p_q := 7236\ Pa$

Absolute pressure at Venturi nozzle:

$$p_V := p_{amb.} + p_2 + p_{12} = \left(2.88924 \cdot 10^5\right)\ Pa$$

Density of water at Venturi nozzle: $\rho_V := 998.764\ \frac{kg}{m^3}$

Venturi flow coefficient: $C := 1.037057$

Reference diameter of Venturi nozzle: $D_V := 0.260\ m$

Test point discharge:

$$Q_{TP} := C \cdot {D_V}^2 \cdot \frac{\pi}{4} \cdot \left(2 \cdot \frac{p_q}{\rho_V}\right)^{0.5} = 0.20959\ \frac{m^3}{s}$$

Specific hydraulic energy
(the term with ζ-values considers the losses between measuring and reference sections)

Test point specific hydraulic energy:

$$E_{h.TP} := \frac{p_{12}}{\frac{\rho_1+\rho_2}{2}} + \frac{\left(\frac{Q_{TP}}{A_1}\right)^2 - \left(\frac{Q_{TP}}{A_2}\right)^2}{2} + \frac{\zeta_1 \cdot \left(\frac{Q_{TP}}{A_1}\right)^2 + \zeta_2 \cdot \left(\frac{Q_{TP}}{A_2}\right)^2}{2} = 96.62547 \ \frac{m^2}{s^2}$$

Mechanical power calculation from lever arm force measurements

Model lever arm force: $F_L := 105.4386 \ N$

Model lenght of lever arm: $R_L := 1.78015 \ m$

Preloading: $m_{load} := 0 \ kg$

Test point torque: $T_{m.TP} := \left(F_L + m_{load} \cdot g\right) \cdot R_L = 187.69652 \ N \cdot m$

Test point mechanical power: $P_{m.TP} := T_{m.TP} \cdot 2 \cdot \pi \cdot n_{TP} = \left(2.4538 \cdot 10^4\right) \ W$

Test point specific mechanical energy: $E_{m.TP} := \frac{P_{m.TP}}{\rho_1 \cdot Q_{TP}} = 117.22053 \ \frac{m^2}{s^2}$

Calculation of efficiency and Reynolds number

Test point hydraulic power: $P_{h.TP} := \rho_1 \cdot E_{h.TP} \cdot Q_{TP} = \left(2.02268 \cdot 10^4\right) \ W$

Test point Hydraulic efficiency: $\eta_{h.TP} := \frac{P_{h.TP}}{P_{m.TP}} = 0.8243$

Viscosity of water: $t := \frac{\left(t_W - 273.15 \ K\right)}{1 \ K} = 17.56$

$$\nu_W := \exp\left(-16.921 + \left(\frac{396.13}{107.41 + t}\right)\right) \frac{m^2}{s} = \left(1.06642 \cdot 10^{-6}\right) \frac{m^2}{s}$$

Test point Reynolds number: $Re_{TP} := \frac{{D_M}^2 \cdot \pi \cdot n_{TP}}{\nu_W} = 5.43481 \cdot 10^6$

3. Data scaling to constant shaft speed of 1450 rpm

The scaled data at constant shaft speed will be used during the following calculations and is therefore defined as "model data" with the subscript "M".

Constant shaft speed: $n_M := \frac{1450}{60}\ \frac{1}{s} = 24.16667\ \frac{1}{s}$

Water density: $\rho_W := 998.2\ \frac{kg}{m^3} = 998.2\ \frac{kg}{m^3}$

Ambient pressure: $p_{amb} := 101325\ Pa$

Discharge: $Q_M := Q_{TP} \cdot \frac{n_M}{n_{TP}} = 0.24344\ \frac{m^3}{s}$

Specific hydraulic energy: $E_{h.M} := E_{h.TP} \cdot \left(\frac{n_M}{n_{TP}}\right)^2 = 130.35272\ \frac{m^2}{s^2}$

Head: $H_M := \frac{E_{h.M}}{g} = 13.29176\ m$

Specific speed: $N_{QE} := n_M \cdot \frac{Q_M^{0.5}}{E_{h.M}^{0.75}} = 0.30908$

Reynolds number: $Re_M := 6707519$

The model pressure at low pressure section is determined through the equal Thoma number σ of the model at tested and at constant shaft speed.

$$\sigma = \frac{NPSE_M}{E_{h.M}} = \frac{NPSE_{TP}}{E_{h.TP}} \quad \text{with} \quad NPSE = \frac{p_2 + p_{amb} - p_v}{\rho(p_2, t_w)} + \frac{\left(\frac{Q}{A_2}\right)^2}{2}$$

Vapour pressure at cavitation section: $p_{v.tw} := 2163\ Pa$

Vapour pressure at cavitation section for 1450 rpm: $p_{v.M} := 2337\ Pa$

Pressure at low pressure section:

$$p_{2.M} := \left(\left(\frac{p_2 + p_{amb.} - p_{v.tw}}{\rho_2} + \frac{\left(\frac{Q_{TP}}{A_2}\right)^2}{2}\right) \cdot \frac{E_{h.M}}{E_{h.TP}} - \frac{\left(\frac{Q_M}{A_2}\right)^2}{2}\right) \cdot \rho_W + p_{v.M} - p_{amb}$$

$$p_{2.M} = \left(1.65405 \cdot 10^5\right)\ Pa$$

Differential pressure between high and low pressure section:

$$p_{12.M} := \left(E_{h.M} - \frac{\left(\frac{Q_M}{A_1}\right)^2 - \left(\frac{Q_M}{A_2}\right)^2}{2} - \frac{\zeta_1 \cdot \left(\frac{Q_M}{A_1}\right)^2 + \zeta_2 \cdot \left(\frac{Q_M}{A_2}\right)^2}{2} \right) \cdot \rho_W$$

$$p_{12.M} = \left(1.22257 \cdot 10^5\right) \; Pa$$

Calculation of efficiency
(the efficiency is scaled to the constant shaft speed of 1450 rpm by utilizing the scale-up formula presented in the standard IEC 60193)

Efficiency at optimum point: $\eta_{opt} := 0.82579$

Reynolds nuber at optimum point: $Re_{opt} := 5619775$

Loss distribution coefficient: $V_{ref} := 0.6$

Relative scalable loss: $$\delta_{ref} := \frac{1 - \eta_{opt}}{\left(\frac{Re_{ref}}{Re_{opt}}\right)^{0.16} + \frac{1 - V_{ref}}{V_{ref}}} = 0.10233$$

Efficiency difference: $$\Delta\eta_{h.TP\_M} := \delta_{ref} \cdot \left(\left(\frac{Re_{ref}}{Re_{TP}}\right)^{0.16} - \left(\frac{Re_{ref}}{Re_M}\right)^{0.16} \right) = 0.00353$$

Model efficiency: $\eta_{h.M} := \eta_{h.TP} + \Delta\eta_{h.TP\_M} = 0.82783$

4. Runner (RU) scale-up coefficients

4.1 Runner blades (RB):

The friction losses for the runner blades are determined with the friction coefficient of a flat plate. The utilized relative velocity is an average of the relative velocities at the inner and outer diameter of the runner inlet and outlet.

4.1.1 Runner blades dimensions:

Average runner blade width:

Average value of the runner blade width, determined by averaging the blade width at the impeller inlet and outlet.

$$B_{RB} := \frac{(0.30973 - 0.1973) + (0.28581 - 0.1184)}{4} \cdot m = 0.06996\ m$$

Runner blade length: $L_{RB} := 0.220\ m$

Number of runner blades: $Z_{RB} := 5$

Diameters and areas: $D_{RU.out.ext} := 0.30973\ m$ $D_{RU.out.int} := 0.198\ m$

$D_{RU.in.ext} := 0.28581\ m$ $D_{RU.in.int} := 0.1184\ m$

Cross sectional area of the flow in the annular runner channel at the outlet and inlet

$$A_{RU.out} := \frac{\left(D_{RU.out.ext}^{\ 2} - D_{RU.out.int}^{\ 2}\right) \cdot \pi}{4} = 0.04455\ m^2$$

$$A_{RU.in} := \frac{\left(D_{RU.in.ext}^{\ 2} - D_{RU.in.int}^{\ 2}\right) \cdot \pi}{4} = 0.05315\ m^2$$

4.1.2 Runner blades velocities:

	Velocities		Subscripts
u	= peripheral velocity	ext	= at external diameter
c_u	= absolute flow velocity	int	= at internal diameter
c_m	= absolute meridian flow velocity	out	= at runner outlet
c	= absolute flow velocity	in	= at runner inlet
w	= relative flow velocity		

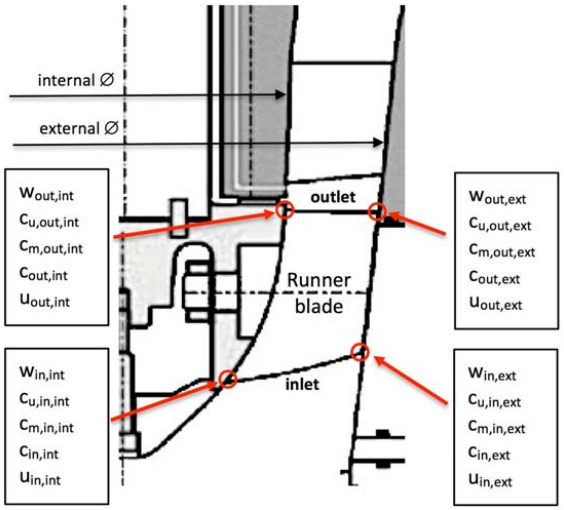

Peripheral outlet velocity at D_{ext}:

$$u_{out.ext} := 2 \cdot \pi \cdot n_M \cdot \frac{D_{RU.out.ext}}{2} = 23.51527 \ \frac{m}{s}$$

Peripheral outlet velocity at D_{int}:

$$u_{out.int} := 2 \cdot \pi \cdot n_M \cdot \frac{D_{RU.out.int}}{2} = 15.03252 \ \frac{m}{s}$$

Peripheral inlet velocity at D_{ext}:

$$u_{in.ext} := 2 \cdot \pi \cdot n_M \cdot \frac{D_{RU.in.ext}}{2} = 21.69922 \ \frac{m}{s}$$

Peripheral inlet velocity at D_{int}:

$$u_{in.int} := 2 \cdot \pi \cdot n_M \cdot \frac{D_{RU.in.int}}{2} = 8.98914 \ \frac{m}{s}$$

Absolut peripheral outlet velocity at D_{ext}:

$$c_{u\_out.ext} := \frac{g \cdot H_M}{u_{out.ext}} \cdot \frac{1}{\eta_{h.M}} = 6.69619 \ \frac{m}{s}$$

Absolut peripheral outlet velocity at D_{int}:

$$c_{u\_out.int} := \frac{g \cdot H_M}{u_{out.int}} \cdot \frac{1}{\eta_{h.M}} = 10.4748 \ \frac{m}{s}$$

Absolut outlet meridian velocity: $$c_{m\_out} := \frac{Q_M}{A_{RU.out}} = 5.46379 \ \frac{m}{s}$$

Absolut inlet meridian velocity: $$c_{m\_in} := \frac{Q_M}{A_{RU.in}} = 4.58045 \ \frac{m}{s}$$

Absolute outlet velocity at D_{ext}:

$$c_{out.ext} := \sqrt{{c_{m\_out}}^2 + {c_{u\_out.ext}}^2} = 8.64245 \ \frac{m}{s}$$

Absolute outlet velocity at D_{int}:

$$c_{out.int} := \sqrt{{c_{m\_out}}^2 + {c_{u\_out.int}}^2} = 11.81416 \ \frac{m}{s}$$

The absolute flow velocity at the runner inlet is assumed to be purely axial

Absolute inlet velocity at D_{ext}: $$c_{in.ext} := c_{m\_in} = 4.58045 \ \frac{m}{s}$$

Absolute inlet velocity at D_{int}: $$c_{in.int} := c_{m\_in} = 4.58045 \ \frac{m}{s}$$

External outlet relative velocity angle:

$$\beta_{out.ext} := \operatorname{atan}\left(\frac{c_{m\_out}}{u_{out.ext} - c_{u\_out.ext}}\right) = 0.3141$$

Internal outlet relative velocity angle:

$$\beta_{out.int} := \operatorname{atan}\left(\frac{c_{m\_out}}{u_{out.int} - c_{u\_out.int}}\right) = 0.87557$$

External inlet relative velocity angle:

$$\beta_{in.ext} := \operatorname{atan}\left(\frac{c_{m\_in}}{u_{in.ext}}\right) = 0.20803$$

Internal inlet relative velocity angle:

$$\beta_{in.int} := \operatorname{atan}\left(\frac{c_{m\_in}}{u_{in.int}}\right) = 0.47126$$

External outlet relative velocity: $w_{out.ext} := \frac{c_{m\_out}}{\sin(\beta_{out.ext})} = 17.6843 \ \frac{m}{s}$

Internal outlet relative velocity: $w_{out.int} := \frac{c_{m\_out}}{\sin(\beta_{out.int})} = 7.11518 \ \frac{m}{s}$

External inlet relative velocity: $w_{in.ext} := \frac{c_{m\_in}}{\sin(\beta_{in.ext})} = 22.17739 \ \frac{m}{s}$

Internal inlet relative velocity: $w_{in.int} := \frac{c_{m\_in}}{\sin(\beta_{in.int})} = 10.08887 \ \frac{m}{s}$

Averaged relative velocity calculated with the relative flow velocity at the inner (int) and outer (ext) diameter of the impeller inlet (in) and outlet (out).

Average relative velocity:

$$w := \frac{w_{in.int} + w_{in.ext} + w_{out.int} + w_{out.ext}}{4} = 14.26643 \ \frac{m}{s}$$

4.1.3 Runner blades dimension factor:

$\kappa_{d.RU}$ = Runner blade length divided by the reference diameter of the RCP

Dimension factor: $\kappa_{d.RU} := \frac{L_{RB}}{D_M} = 0.73883$

4.1.4 Runner blades flow velocity factor:

Reference peripheral velocity: $u := 2 \cdot \pi \cdot n_M \cdot \frac{D_M}{2} = 22.60724 \ \frac{m}{s}$

$\kappa_{d.RU}$ = Runner blade average relative velocity divided by the reference peripheral velocity

Flow velocity factor: $\kappa_{u.RU} := \frac{w}{u} = 0.63106$

4.1.5 Friction loss coefficient for runner blades:

Friction loss coefficient of a flat plate (IEC 62097):

Friction coefficient of a flat plate according to IEC 62097, with Ra_{RB} = surface roughness of the runner blades and Re_{ref} = reference Reynolds number ($7 \cdot 10^6$ acc. to IEC)

$$C_{f.RU} := 0.0032 \cdot \left(0.80 \cdot \left(5 \cdot 10^5 \cdot \frac{Ra_{RB}}{L_{RB}} + \frac{Re_{ref}}{\kappa_{d.RU} \cdot \kappa_{u.RU} \cdot Re_M} \right)^{0.2} + 0.20 \right)$$

$$C_{f.RU} = 0.00391$$

4.1.6 Friction loss coefficient at reference condition:

The friction coefficient at reference condition is calculated by considering a model with smooth surfaces and with Reynolds number equal to Re_{ref}. With these considerations, the friction coefficent formula simplifies to the form presented below.

Friction loss coefficient of a flat plate (IEC 62097):

$$C_{f.RU.ref} := 0.0032 \cdot \left(0.80 \cdot \left(\frac{1}{\kappa_{d.RU} \cdot \kappa_{u.RU}} \right)^{0.2} + 0.20 \right) = 0.00362$$

4.1.7 Friction specific hydraulic energy loss at the blades suction and pressure side:

For the Type 1134 RCP Andritz AG provided the relative velocity distribution along the pressure and suction side of the runner blades, which allowed a separate calculation of the friction losses of each blade side.

A_{RU} = average cross sectional area of the flow in the annular runner channel
(annular inlet area + annular outlet area)/2

$$A_{RU} := \frac{\left(\frac{\left(0.30973^2 - 0.198^2\right)\cdot\pi}{4} + \frac{\left(0.28581^2 - 0.1184^2\right)\cdot\pi}{4}\right)}{2} m^2 = 0.04885\ m^2$$

Average relative velocity for the suction and pressure side of the runner blades and the therewith calculated velocity factor for each blade side.

$$w_{SS} := 15.46049\ \frac{m}{s} \qquad \kappa_{u.RU\_SS} := \frac{w_{SS}}{u} = 0.68387$$

$$w_{PS} := 11.20679\ \frac{m}{s} \qquad \kappa_{u.RU\_PS} := \frac{w_{PS}}{u} = 0.49572$$

Friction factor for each blade side

$$C_{f.RU\_SS} := 0.0032\cdot\left(0.80\cdot\left(5\cdot10^5\cdot\frac{Ra_{RB}}{L_{RB}} + \frac{Re_{ref}}{\kappa_{d.RU}\cdot\kappa_{u.RU\_SS}\cdot Re_M}\right)^{0.2} + 0.20\right)$$

$$C_{f.RU\_SS} = 0.00387$$

$$C_{f.RU\_PS} := 0.0032\cdot\left(0.80\cdot\left(5\cdot10^5\cdot\frac{Ra_{RB}}{L_{RB}} + \frac{Re_{ref}}{\kappa_{d.RU}\cdot\kappa_{u.RU\_PS}\cdot Re_M}\right)^{0.2} + 0.20\right)$$

$$C_{f.RU\_PS} = 0.00402$$

Friction force equation for a flat plate (K.-H. Grote, J. Feldhusen; DUBBEL-Taschenbuch für Maschinenbau; Springer; 2012):

$$F_r = C_r \cdot \left(\rho \cdot \frac{v^2}{2}\right) \cdot S_0 \qquad \text{with} \qquad S_0 = \text{blade surface} = L_{RB} \cdot B_{RB}$$

Energy loss due to friction:

$$E = \frac{\Delta p}{\rho} = \frac{F_r}{A \cdot \rho} \qquad \text{with} \qquad A = \text{sectional area of the flow for one blade} = \frac{A_{RU}}{Z_{RB}}$$

The equation is then multiplied by the number of blades Z_{RB}, since each blade has a suction/pressure side.

$$E_{Lf.RB\_SS} := C_{f.RU\_SS} \cdot \frac{L_{RB} \cdot B_{RB}}{\frac{A_{RU}}{Z_{RB}}} \cdot \frac{w_{SS}^2}{2} \cdot Z_{RB} = 3.6439 \ \frac{m^2}{s^2}$$

$$E_{Lf.RB\_PS} := C_{f.RU\_PS} \cdot \frac{L_{RB} \cdot B_{RB}}{\frac{A_{RU}}{Z_{RB}}} \cdot \frac{w_{PS}^2}{2} \cdot Z_{RB} = 1.98618 \ \frac{m^2}{s^2}$$

4.2 Annular runner channel (RUC):

The inner wall of the annular runner channel moves at the rotational speed of the runner, while the outer wall is stationary. In order avoid a further component subdivision to calculate these minor losses, the moving inner surface is not considered, as it is considerably smaller compared to the outer surface.

4.2.1 Annular runner channel geometry:

Since the flow inside the runner channel has a peripheral velocity, a fluid particle traveling along the outer channel surface covers a longer distance than the axial length of the channel. The distance covered by the fluid particle at the outer channel wall is, therefore, determined by calculating the hypotenuse of the triangle having length equal to the peripheral distance traveled and height equal to the axial channel length.

Axial length of the runner channel: $L_{RUC.m} := 2 \cdot 0.0569\ m = 0.1138\ m$

Time needed for a water particle to flow through the channel at average meridian velocity:

$$t := \frac{L_{RUC.m}}{\frac{\left(c_{m\_out} + c_{m\_in}\right)}{2}} = 0.02266\ s$$

Peripheral distance traveled in this time at average peripheral velocity:

$c_{u\_in.ext} := 0\ \frac{m}{s}$

$L_{RUC.u} := \frac{\left(c_{u\_out.ext} + c_{u\_in.ext}\right)}{2} \cdot t = 0.07587\ m$

Flow length of runner channel: $L_{RUC} := \sqrt{{L_{RUC.u}}^2 + {L_{RUC.m}}^2} = 0.13677\ m$

4.2.2 Hydraulic diameter:

Hydraulic diameter of the runner channel:

$$d_{h.RUC} := \frac{D_{RU.in.ext} + D_{RU.out.ext}}{2} = 0.29777\ m$$

4.2.3 Dimension factor:

Dimension factor of the runner channel: $\kappa_{d.RUC} := \frac{d_{h.RUC}}{D_M} = 1$

4.2.4 Mean velocity in flow passage:

Since the losses are calculated only for the outer channel wall, the averaged channel velocity is set equal to the velocity, obtained by averaging absolute velocity of the inlet and outlet at the outer diameter.

Mean velocity in runner channel:

$$v_{RUC} := \frac{c_{out.ext} + c_{in.ext}}{2} = 6.61145 \ \frac{m}{s}$$

4.2.5 Flow velocity factor:

Flow velocity factor of the runner channel:

$$\kappa_{u.RUC} := \frac{v_{RUC}}{u} = 0.29245$$

4.2.6 Friction loss coefficients:

The friction coefficient is calculated by using the explicit formula for pipe friction according to IEC 62097.

Friction loss coefficient for runner channel (IEC 62097) :

$$\lambda_{RUC} := 0.0085 \cdot \left(0.74 \cdot \left(4 \cdot 10^5 \cdot \frac{Ra_{RUC}}{\kappa_{d.RUC} \cdot D_M} + \frac{Re_{ref}}{\kappa_{u.RUC} \cdot \kappa_{d.RUC} \cdot Re_M} \right)^{0.2} + 0.26 \right) = 0.01076$$

4.2.7 Friction loss of specific hydraulic energy:

The energy loss due to friction is calculated by using the formula for pipe friction losses according to IEC 62097.

Friction loss of specific hydraulic energy at the runner channel:

$$E_{Lf.RUC} := \lambda_{RUC} \cdot \frac{L_{RUC}}{d_{h.RUC}} \cdot \frac{{v_{RUC}}^2}{2} = 0.10803 \ \frac{m^2}{s^2}$$

4.3 Scalable hydraulic energy loss index for the runner:

Total specific hydraulic energy loss due to friction in the runner:

The total energy loss is equal to the sum of the losses due to friction of the pressure and suction side of the runner blades, and the friction losses of the runner channel.

$$E_{Lf.RU} := E_{Lf.RB\_SS} + E_{Lf.RB\_PS} + E_{Lf.RUC} = 5.7381 \ \frac{m^2}{s^2}$$

Relative scalable hydraulic energy loss:

$$\delta_{E.RU} := \frac{E_{Lf.RU}}{E_{h.M}} = 0.04402$$

Reference scalable hydraulic energy loss:

To obtain a scalable energy loss index applicable to all axial working RCPs, it is necessary to convert the relative scalable energy loss to the relative energy loss at reference condition. This is achived by mutiplying the relative energy loss by the ratio of the reference friction coefficient to the regular friction coefficient.

$$\delta_{E.RU.ref} := \delta_{E.RU} \ \frac{C_{f.RU.ref}}{C_{f.RU}} = 0.04083$$

Scalable hydraulic energy loss index:

$$d_{E.RU.ref} := \frac{\delta_{E.RU.ref}}{1 + 0.25 \cdot \left(\kappa_{u.RU} \cdot \kappa_{d.RU}\right)^{0.2}} = 0.03362$$

5. Guide vane section (GVS) scale-up coefficients

For the guide vane section the same procedure and friction formulas used for the runner are adopted. What changes is the geometriy and the relevant velocity.

5.1 Guide vanes (GV):

5.1.1 Guide vane dimensions:

Average guide vane width:

Average value of the runner blade width, determined by averaging the blade width at the impeller inlet and outlet.

$$B_{GV} := \frac{(0.32889 - 0.20366) + (0.3152 - 0.1973)}{4} \cdot m = 0.06078\ m$$

Guide vane length: $L_{GV} := 0.090 \cdot m$

Number of guide vanes: $Z_{GV} := 14$

Diameters: $D_{GV.out.ext} := 0.32889\ m$

$D_{GV.out.int} := 0.20366\ m$

Guide vane outlet area:

Cross sectional area of the flow in the annular guide vane channel outlet

$$A_{GV.out} := \frac{\left(D_{GV.out.ext}^{\ 2} - D_{GV.out.int}^{\ 2}\right) \cdot \pi}{4} = 0.05238\ m^2$$

5.1.2 Dimension factor:

Dimension factor: $\kappa_{d.GV} := \frac{L_{GV}}{D_M} = 0.30225$

5.1.3 Guide vane velocities:

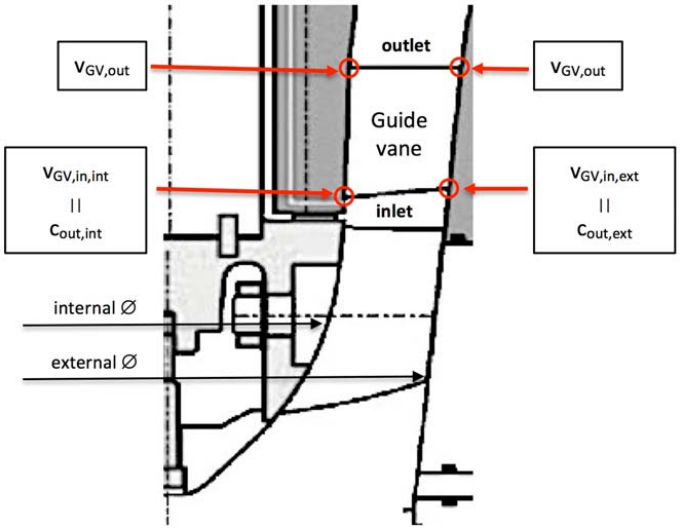

Average guide vane inlet velocity: $$v_{GV.in} := \frac{c_{out.ext} + c_{out.int}}{2} = 10.22831 \ \frac{m}{s}$$

At the guide vane channel inlet the velocity is assumed to be equal to the runner outlet velocity.

Average guide vane outlet velocity: $$v_{GV.out} := \frac{Q_M}{A_{GV.out}} = 4.64759 \ \frac{m}{s}$$

At the guide vane channel outlet it is assumed that the flow velocity is purely axial and can therefore be determined by dividing the discharge by the cross sectional area of the flow at the outlet.

Average guide vane velocity: $$v_{GV} := \frac{v_{GV.in} + v_{GV.out}}{2} = 7.43795 \ \frac{m}{s}$$

5.1.4 Flow velocity factor:

Flow velocity factor: $$\kappa_{u.GV} := \frac{v_{GV}}{u} = 0.32901$$

The following calculation of the energy loss due to friction of the guide vanes (friction on flat plates) is identical to the calculation carried out for the runner blades, with the values of the guide vanes.

5.1.5 Friction loss coefficient:

Friction loss coefficient of a flat plate (IEC 62097):

$$C_{f.GV} := 0.0032 \cdot \left(0.80 \cdot \left(5 \cdot 10^{5} \cdot \frac{Ra_{GV}}{L_{GV}} + \frac{Re_{ref}}{\kappa_{d.GV} \cdot \kappa_{u.GV} \cdot Re_{M}}\right)^{0.2} + 0.20\right)$$

$$C_{f.GV} = 0.00493$$

5.1.6 Friction loss coefficient at reference condition:

Friction loss coefficient of a flat plate (IEC 62097):

$$C_{f.GV.ref} := 0.0032 \cdot \left(0.80 \cdot \left(\frac{1}{\kappa_{d.GV} \cdot \kappa_{u.GV}}\right)^{0.2} + 0.20\right) = 0.0047$$

5.1.7 Friction specific hydraulic energy loss at the vanes suction and pressure side:

For the Type 1134 RCP Andritz AG provided the relative velocity distribution along the pressure and suction side of the guide vanes, which allowed a separate calculation of the friction losses of each vane side.

$$A_{GV} := \left(\frac{0.32889^2 - 0.20366^2}{4} + \frac{0.3152^2 - 0.1973^2}{4}\right) \cdot \frac{\pi}{2}\ m^2 = 0.04992\ m^2$$

A_{GV} = average cross sectional area of the flow in the annular guide vane channel (annular inlet area + annular outlet area)/2

$$v_{GV\_SS} := 7.94865\ \frac{m}{s} \qquad \kappa_{u.GV\_SS} := \frac{v_{GV\_SS}}{u} = 0.3516$$

$$v_{GV\_PS} := 5.45712\ \frac{m}{s} \qquad \kappa_{u.GV\_PS} := \frac{v_{GV\_PS}}{u} = 0.24139$$

Average flow velocity for the suction and pressure side of the guide vanes and the therewith calculated velocity factor for each vane side.

Friction factor and specific energy loss due to friction for each vane side

$$C_{f.GV\_SS} := 0.0032 \cdot \left(0.80 \cdot \left(5 \cdot 10^5 \cdot \frac{Ra_{GV}}{L_{GV}} + \frac{Re_{ref}}{\kappa_{d.GV} \cdot \kappa_{u.GV\_SS} \cdot Re_M}\right)^{0.2} + 0.20\right)$$

$$C_{f.GV\_SS} = 0.00489$$

$$C_{f.GV\_PS} := 0.0032 \cdot \left(0.80 \cdot \left(5 \cdot 10^5 \cdot \frac{Ra_{GV}}{L_{GV}} + \frac{Re_{ref}}{\kappa_{d.GV} \cdot \kappa_{u.GV\_PS} \cdot Re_M}\right)^{0.2} + 0.20\right)$$

$$C_{f.GV\_PS} = 0.00516$$

$$E_{Lf.GV\_SS} := C_{f.GV\_SS} \cdot \frac{L_{GV} \cdot B_{GV}}{\frac{A_{GV}}{Z_{GV}}} \cdot \frac{{v_{GV\_SS}}^2}{2} \cdot Z_{GV} = 3.31749 \ \frac{m^2}{s^2}$$

$$E_{Lf.GV\_PS} := C_{f.GV\_PS} \cdot \frac{L_{GV} \cdot B_{GV}}{\frac{A_{GV}}{Z_{GV}}} \cdot \frac{{v_{GV\_PS}}^2}{2} \cdot Z_{GV} = 1.64901 \ \frac{m^2}{s^2}$$

5.2 Annular guide vane channel (GVC):

The annular guide vane channel walls are both stationary, which allows the calculation of friction losses with the formulas for annular channels.

5.2.1 Annular guide vane channel geometry:

Average area of the flow at the guide vane channel:

$$A_{GVC} := \left(\frac{0.32889^2 - 0.20366^2}{4} + \frac{0.3152^2 - 0.1973^2}{4} \right) \cdot \frac{\pi}{2}\ m^2 = 0.04992\ m^2$$

A_{GVC} = average cross sectional area of the flow in the annular guide vane channel (annular inlet area + annular outlet area)/2

Average wetted perimeter of the guide vane channel:

$$P_{GVC} := \left((0.32889 + 0.20366) + (0.3152 + 0.1973) \right) \cdot \frac{\pi}{2}\ m = 1.64156\ m$$

Length of guide vane channel: $L_{GVC} := 0.090 \cdot m$

5.2.2 Hydraulic diameter:

Hydraulic diameter of guide vane channel:

$$d_{h.GVC} := \frac{4 \cdot A_{GVC}}{P_{GVC}} = 0.12164\ m$$

$\frac{4 \cdot A}{P}$ = global formulation for the hydraulic diameter

5.2.3 Dimension factor:

Dimension factor of guide vane section: $\kappa_{d.GVC} := \frac{d_{h.GVC}}{D_M} = 0.40849$

5.2.4 Mean velocity in the flow passage:

Mean velocity in the guide vane channel: $v_{GVC} := v_{GV} = 7.43795\ \frac{m}{s}$

The mean velocity in the guide vane channel is equal to the average flow velocity of the guide vanes.

5.2.5 Flow velocity factor:

Peripheral velocity at the reference diameter:

$$u := D_M \cdot \pi \cdot n_M = 22.60724 \ \frac{m}{s}$$

Flow velocity factor of the guide vane channel:

$$\kappa_{u.GVC} := \frac{v_{GVC}}{u} = 0.32901$$

5.2.6 Friction loss coefficients:

The friction coefficient is calculated by using the explicit formula for pipe friction according to IEC 62097.

Friction loss coefficient (IEC 62097) of the guide vane channel:

$$\lambda_{GVC} := 0.0085 \cdot \left(0.74 \cdot \left(4 \cdot 10^5 \cdot \frac{Ra_{GVC}}{\kappa_{d.GVC} \cdot D_M} + \frac{Re_{ref}}{\kappa_{u.GVC} \cdot \kappa_{d.GVC} \cdot Re_M} \right)^{0.2} + 0.26 \right) = 0.01292$$

5.2.7 Friction loss of specific hydraulic energy:

Friction loss of specific hydraulic energy at the guide vane channel:

$$E_{Lf.GVC} := \lambda_{GVC} \cdot \frac{L_{GVC}}{d_{h.GVC}} \cdot \frac{{v_{GVC}}^2}{2} = 0.26453 \ \frac{m^2}{s^2}$$

5.3 Scalable hydraulic energy loss index for the guide vane section:

Total specific hydraulic energy loss due to friction in the guide vane section:

The total energy loss is equal to the sum of the losses due to friction of the pressure and suction side of the guide vanes, and the friction losses of the guide vane channel.

$$E_{Lf\_GVS} := E_{Lf.GV\_SS} + E_{Lf.GV\_PS} + E_{Lf.GVC} = 5.23104 \ \frac{m^2}{s^2}$$

Relative scalable hydraulic energy loss:

$$\delta_{E.GVS} := \frac{E_{Lf\_GVS}}{E_{h.M}} = 0.04013$$

Reference scalable hydraulic energy loss:

$$\delta_{E.GVS.ref} := \delta_{E.GVS} \frac{C_{f.GV.ref}}{C_{f.GV}} = 0.03824$$

Scalable hydraulic energy loss index:

$$d_{E.GVS.ref} := \frac{\delta_{E.GVS.ref}}{1 + 0.25 \cdot \left(\kappa_{u.GV} \cdot \kappa_{d.GV}\right)^{0.2}} = 0.03304$$

6. Cylindrical case (CY) scale-up coefficients

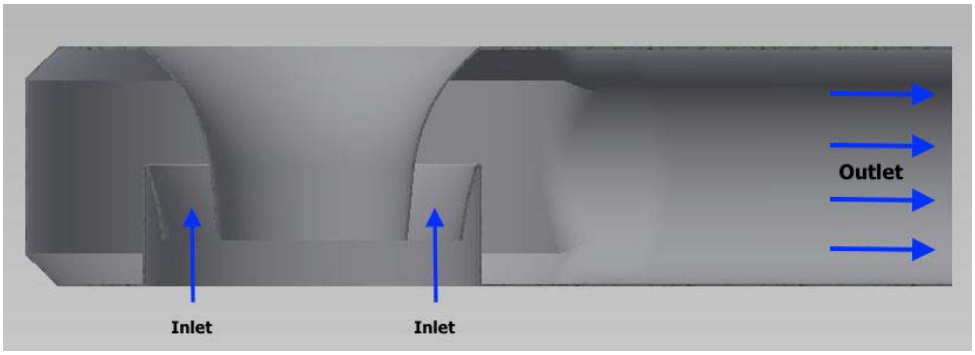

6.1 Cylindrical case geometry:

Average cross-sectional area of the flow at inlet section:

$$A_{CY\_in} := \left(\frac{\left(0.32889^2 - 0.20366^2\right)}{4} + \frac{\left(0.36366^2 - 0.2194^2\right)}{4} \right) \cdot \frac{\pi}{2} \cdot m^2 = 0.05922\ m^2$$

Average cross sectional area of the flow at the annular casing inlet, necessary to calculate a representative cross sectional area of the flow for the entire cylindrical casing.

Average cross sectional area of the flow at outlet section:

Cross sectional area of the flow at the elliptical part of the casing outlet, where the outlet pipe connects to the cylindical part of the casing.

$$A_{CY\_out.1} := 0.13085 \cdot \cos\left(\frac{20 \cdot \pi}{180}\right) \cdot \frac{0.2617}{2} \cdot \pi + 0.2617 \cdot 2 \cdot (0.3594 - 0.279) \cdot \tan\left(\frac{20 \cdot \pi}{180}\right)$$

Cross sectional area of the flow of the outlet pipe

$$A_{CY\_out.2} := \frac{0.2436^2 \cdot \pi}{4}$$

Average cross sectional area of the flow at outlet section

$$A_{CY\_out} := \frac{\left(A_{CY\_out.1} + A_{CY\_out.2}\right)}{2}\ m^2 = 0.05623\ m^2$$

Average cross-sectional area of the flow at cylindrical part:

$$A_{CY\_cy} := \left((0.628 - 0.3664) \cdot 0.2617 - 4 \cdot \frac{0.035^2}{2} \right) m^2 = 0.06601\ m^2$$

Average cross-sectional area of the flow for the whole casing:

Representative cross-sectional area of the flow for the whole casing, used to obtain the energy loss due to friction from the wall shear force, determined through the CFD-analysis.

$$A_{CY} := \frac{A_{CY\_in} + A_{CY\_out} + A_{CY\_cy}}{3} = 0.06049\ m^2$$

6.2 Hydraulic diameter:

The representative hydraulic diameter for the casing is defined as the average of the inlet, outlet, and cylindrical part of the casing.

Average perimeter of the annular inlet section:

$$P_{CY\_in} := ((0.32889 + 0.20366) + (0.36366 + 0.2194)) \cdot \frac{\pi}{2} \cdot m = 1.7524\ m$$

Average perimeter of the outlet section (elliptical connection & outlet pipe):

$$P_{CY\_out.1} := \left(\pi \cdot \sqrt{2 \cdot \left(\left(0.13085 \cdot \cos\left(\frac{20 \cdot \pi}{180} \right) \right)^2 + \left(\frac{0.2617}{2} \right)^2 \right)} + 4 \cdot 0.0804 \cdot \tan\left(\frac{20 \cdot \pi}{180} \right) \right) m$$

$$P_{CY\_out.2} := 0.2436 \cdot \pi \cdot m$$

$$P_{CY\_out} := \frac{P_{CY\_out.1} + P_{CY\_out.2}}{2} = 0.84005\ m$$

Average perimeter of the cylindrical part:

$$P_{CY\_cy} := 2 \cdot \left(0.2617 - 2 \cdot 0.035 + 2 \cdot \sqrt{2} \cdot 0.035 + 2 \cdot \left(\frac{0.628 - 0.3664}{2} - 0.035 \right) + \frac{0.2617}{2} \right) m$$

$$P_{CY\_cy} = 1.22629\ m$$

Hydraulic diameter of inlet section: $d_{h.CY\_in} := \frac{4 \cdot A_{CY\_in}}{P_{CY\_in}} = 0.13518\ m$

Hydraulic diameter of outlet section: $d_{h.CY\_out} := \frac{4 \cdot A_{CY\_out}}{P_{CY\_out}} = 0.26777\ m$

Hydraulic diameter of cylindrical part: $d_{h.CY\_cy} := \frac{4 \cdot A_{CY\_cy}}{P_{CY\_cy}} = 0.21532\ m$

Average hydraulic diameter:

The representative hydraulic diameter of the casing is necessary to determine the dimension factor κ_d for the casing.

$$d_{h.CY} := \frac{d_{h.CY\_in} + d_{h.CY\_out} + d_{h.CY\_cy}}{3} = 0.20609\ m$$

6.3 Dimension factor:

Dimension factor: $\kappa_{d.CY} := \frac{d_{h.CY}}{D_M} = 0.6921$

6.4 Mean velocity in flow passage:

The mean flow velocity in the cylindrical casing was obtained from the CFD-analysis of the casing.

Mean velocity in flow passage: $v_{CY} := 3.70671\ \frac{m}{s}$

6.5 Flow velocity factor:

Peripheral velocity at the reference diameter: $u := D_M \cdot \pi \cdot n_M = 22.60724\ \frac{m}{s}$

Flow velocity factor: $\kappa_{u.CY} := \frac{v_{CY}}{u} = 0.16396$

6.6 Friction loss coefficients:

The friction coefficients are not directly utilized to determine the friction losses in the cylindrical casing, but to convert the relative scalable losses to reference scalable losses.
The friction coefficients are calculated by using the explicit formula for pipe friction, according to IEC 62097.

Friction loss coefficient (IEC 62097):

$$\lambda_{CY} := 0.0085 \cdot \left(0.74 \cdot \left(4 \cdot 10^5 \cdot \frac{Ra_{CY}}{\kappa_{d.CY} \cdot D_M} + \frac{Re_{ref}}{\kappa_{u.CY} \cdot \kappa_{d.CY} \cdot Re_M}\right)^{0.2} + 0.26\right) = 0.01273$$

Friction loss coefficient at reference condition (IEC 62097):

$$\lambda_{CY.ref} := 0.0085 \cdot \left(0.74 \cdot \left(\frac{1}{\kappa_{u.CY} \cdot \kappa_{d.CY}}\right)^{0.2} + 0.26\right) = 0.01193$$

6.7 Friction loss of specific hydraulic energy:

The wall friction force in the cylindrical casing was determined by integrating the wall shear stress over the surface of the cylindrical casing in the CFD-analysis.

Friction force on the walls:

$$F_{f.CY} := 2 \cdot 28.02090\ N = 56.0418\ N$$

The obtained wall friction force is multiplied by 2, since only the symmetric half of the cylindrical casing was simulated.

Friction loss of specific hydraulic energy:

The specific energy loss due to friction is obtained by dividing the wall friction force by the cross sectional area of the flow and the density.

Energy loss for a channel:

$$\Delta p \cdot A = \int \tau_W \, dS_W = F_W \quad \text{with} \quad E_{Lf} = \frac{\Delta p}{\rho} \quad => \quad E_{Lf} = \frac{F_W}{A \cdot \rho}$$

$$E_{Lf.CY} := \frac{F_{f.CY}}{A_{CY} \cdot \rho_W} = 0.92816\ \frac{m^2}{s^2}$$

6.8 Scalable hydraulic energy loss index:

Relative scalable hydraulic energy loss:

$$\delta_{E.CY} := \frac{E_{Lf.CY}}{E_{h.M}} = 0.00712$$

Reference scalable hydraulic energy loss:

$$\delta_{E.CY.ref} := \delta_{E.CY} \frac{\lambda_{CY.ref}}{\lambda_{CY}} = 0.00667$$

Scalable hydraulic energy loss index:

$$d_{E.CY.ref} := \frac{\delta_{E.CY.ref}}{1 + 0.351 \cdot \left(\kappa_{u.CY} \cdot \kappa_{d.CY}\right)^{0.2}} = 0.00544$$

Appendix B

Performance scale-up of the Type 1400 RCP

1. Model data

Reference diameter: $D_M := 0.363479\ m$

Shaft speed: $n_M := \frac{999}{60}\ \frac{1}{s} = 16.65\ \frac{1}{s}$

Discharge: $Q_M := 0.398\ \frac{m^3}{s}$

Specific hydraulic energy: $E_M := 149.655\ \frac{m^2}{s^2}$

Hydraulic efficiency: $\eta_{h.M} := 0.824$

Shaft speed at optimum point: $n_{M.opt} := \frac{999}{60}\ \frac{1}{s} = 16.65\ \frac{1}{s}$

Discharge at optimum point: $Q_{M.opt} := 0.398\ \frac{m^3}{s}$

Specific hydraulic energy at optimum point: $E_{M.opt} := 149.655\ \frac{m^2}{s^2}$

Water density: $\rho_M := 998.43\ \frac{kg}{m^3}$

Water temperature: $t_M := 20\ °C$

Water viscosity:

$$\nu_M := \exp\left(-16.921 + \left(\frac{396.13}{107.41 + \frac{t_M - 273.15\ K}{1\ K}}\right)\right)\ \frac{m^2}{s} = \left(1.00361 \cdot 10^{-6}\right)\ \frac{m^2}{s}$$

Mechanical power: $P_{m.M} := \frac{\rho_M \cdot E_M \cdot Q_M}{\eta_{h.M}} = 72.17133\ kW$

Reference Reynolds number: $Re_{ref} := 7 \cdot 10^6$

Reynolds number: $Re_M := \frac{D_M^{\,2} \cdot \pi \cdot n_M}{\nu_M} = 6.88583 \cdot 10^6$

Specific speed: $N_{QE} := n_{M.opt} \cdot \frac{Q_{M.opt}^{\,0.5}}{E_{M.opt}^{\,0.75}} = 0.24549$

Wall roughness of runner: $Ra_{RU.M} := 0.5 \cdot 10^{-6}\ m$

Wall roughness of guide vane section: $Ra_{GVS.M} := 0.5 \cdot 10^{-6}\ m$

Wall roughness of cylindrical casing: $Ra_{CY.M} := 2 \cdot 10^{-6}\ m$

2. Prototype data

Reference diameter: $D_P := 0.89\ m$

Shaft speed: $n_P := \frac{1190}{60}\ \frac{1}{s} = 19.83333\ \frac{1}{s}$

Water density: $\rho_P := 745\ \frac{kg}{m^3}$

Water temperature: $t_P := 290.6\ °C$

Water viscosity:

$$\nu_P := \exp\left(-16.921 + \left(\frac{396.13}{107.41 + \frac{t_P - 273.15\ K}{1\ K}}\right)\right)\ \frac{m^2}{s} = \left(1.21212 \cdot 10^{-7}\right)\ \frac{m^2}{s}$$

Reynolds number: $Re_P := \frac{D_P^{\,2} \cdot \pi \cdot n_P}{\nu_P} = 4.07173 \cdot 10^8$

Wall roughness of runner: $Ra_{RU.P} := 0.8 \cdot 10^{-6}\ m$

Wall roughness of guide vane section: $Ra_{GV.P} := 0.8 \cdot 10^{-6}\ m$

Wall roughness of cylindrical casing: $Ra_{CY.P} := 3.2 \cdot 10^{-6}\ m$

3. Step-up calculation

3.1 Flow velocity factors:

Runner: $\kappa_{u.RU} := -0.2699 \cdot N_{QE} + 0.7145 = 0.64824$

Guide vane section: $\kappa_{u.GVS} := -0.7368 \cdot N_{QE} + 0.5567 = 0.37582$

Cylindrical case: $\kappa_{u.CY} := -0.3936 \cdot N_{QE} + 0.2856 = 0.18897$

3.2 Scalable hydraulic energy loss index:

Runner: $d_{E.ref.RU} := 0.04372 \cdot N_{QE} + 0.02011 = 0.03084$

Guide vane section: $d_{E.ref.GVS} := 0.05457 \cdot N_{QE} + 0.01617 = 0.02957$

Cylindrical case: $d_{E.ref.CY} := 0.02359 \cdot N_{QE} - 0.00185 = 0.00394$

Shroud ring: $d_{T.ref.SR} := 0.00852 = 0.00852$

3.3 Efficiency step-up ratios:

Runner:

$$\Delta_{E.RU} := d_{E.ref.RU} \cdot \left(\left(5 \cdot 10^5 \cdot \kappa_{u.RU} \cdot \frac{Ra_{RU.M}}{D_M} + \frac{Re_{ref}}{Re_M} \right)^{0.2} - \left(5 \cdot 10^5 \cdot \kappa_{u.RU} \cdot \frac{Ra_{RU.P}}{D_P} + \frac{Re_{ref}}{Re_P} \right)^{0.2} \right)$$

$\Delta_{E.RU} = 0.0089$

Guide vane section:

$$\Delta_{E.GVS} := d_{E.ref.GVS} \cdot \left(\left(5 \cdot 10^5 \cdot \kappa_{u.GVS} \cdot \frac{Ra_{GVS.M}}{D_M} + \frac{Re_{ref}}{Re_M} \right)^{0.2} - \left(5 \cdot 10^5 \cdot \kappa_{u.GVS} \cdot \frac{Ra_{GV.P}}{D_P} + \frac{Re_{ref}}{Re_P} \right)^{0.2} \right)$$

$\Delta_{E.GVS} = 0.00992$

Cylindrical case:

$$\Delta_{E.CY} := d_{E.ref.CY} \cdot \left(\left(4 \cdot 10^5 \cdot \kappa_{u.CY} \cdot \frac{Ra_{CY.M}}{D_M} + \frac{Re_{ref}}{Re_M} \right)^{0.2} - \left(4 \cdot 10^5 \cdot \kappa_{u.CY} \cdot \frac{Ra_{CY.P}}{D_P} + \frac{Re_{ref}}{Re_P} \right)^{0.2} \right)$$

$\Delta_{E.CY} = 0.00116$

Total efficiency step-up ratio affecting the specific hydraulic energy:

$$\Delta_E := \Delta_{E.RU} + \Delta_{E.GVS} + \Delta_{E.CY} = 0.01998$$

Efficiency step-up ratio affecting the mechanical power:

$$\Delta_T := d_{T.ref.SR} \cdot \left(\left(\frac{Re_M}{Re_{ref}} \right)^{-0.24} - \left(\frac{D_M}{D_P} \cdot \frac{Re_P}{Re_{ref}} \right)^{-0.24} \right) = 0.00457$$

Efficiency step-up ratio affecting the discharge:

$$\Delta_Q := 0$$

3.4 Prototype performance at tested point:

Hydraulic efficiency:

$$\eta_{h.P} := \eta_{h.M} \cdot (1 + \Delta_E) \cdot (1 + \Delta_T) \cdot (1 + \Delta_Q) = 0.8443$$

Efficiency difference between model and prototype:

$$\Delta\eta_{h.M\_P} := \eta_{h.P} - \eta_{h.M} = 0.0203$$

Discharge:

$$Q_P := Q_M \cdot \frac{n_P}{n_M} \cdot \left(\frac{D_P}{D_M} \right)^3 \cdot (1 + \Delta_Q) = 6.9598 \ \frac{m^3}{s}$$

Specific hydraulic energy:

$$E_P := E_M \cdot \left(\frac{n_P}{n_M} \right)^2 \cdot \left(\frac{D_P}{D_M} \right)^2 \cdot (1 + \Delta_E) = \left(1.29857 \cdot 10^3 \right) \ \frac{m^2}{s^2}$$

Mechanical power:

$$P_{m.P} := P_{m.M} \cdot \frac{\rho_P}{\rho_M} \cdot \left(\frac{n_P}{n_M} \right)^3 \cdot \left(\frac{D_P}{D_M} \right)^5 \cdot \left(\frac{1}{1 + \Delta_T} \right) = \left(7.97482 \cdot 10^3 \right) \ kW$$

References

[1] ANDRITZ AG. personal communication. January 2018.

[2] ASME. Procedure for estimation and reporting of uncertainty due to discretization in cfd applications. *Journal of Fluids Engineering*, 130, July 2008.

[3] F. R. Menter. Zonal two equation k-ω, turbulence models for aerodynamic flows. *AIAA Journal*, July 1993.

[4] International Electrotechnical Commission. Hydraulic machines, radial and axial – performance conversion method from model to prototype. *INTERNATIONAL STANDARD IEC 62097*, Edition 1.0, February 2009.

[5] International Electrotechnical Commission. Hydraulic turbines, storage pumps and pump-turbines- model acceptance tests. *INTERNATIONAL STANDARD IEC 60193*, Second edition, November 1999.

[6] J.- M Chapallaz, P. Eichenberger, G. Fischer. *Manual on Pumps Used as Turbines*, volume 11. Deutsches Zentrum fur Entwicklungstechnologien GATE, 1992.

[7] K.-H. Grote, J. Feldhusen, editor. *Dubbel - Taschenbuch für den Maschinenbau*. Springer, 23 edition, 2012.

[8] K. Saiki, T. Iikura, K. Matsumoto, H. Komita, M. Kobayashi, T. Saito, H. Tanaka. Performance comparison of nuclear reactor recirculation pumps tested under large reynolds number difference. In E. Cabrera, V. Espert, F. Martínez, editor, *Hydraulic Machinery and Cavitation*. Springer Netherlands, 1996.

[9] M. Salim, S.C. Cheah. Wall y+ strategy for dealing with wall-bounded turbulent flows. *Proceedings of the International MultiConference of Engineers and Computer Scientists*, 2009.

[10] H. Oertel. *Prandtl-Führer durch die Strömungslehre. Grundlagen und Phänomene*, volume 13. Springer Vieweg, 2012.

[11] P. J. Roache. A method for uniform reporting of grid refinement studies. *Journal of Fluids Engineering*, 116, September 1994.

[12] Univ.Prof. Dipl.-Ing. Dr.-Ing. C. Bauer. *Hydraulische Maschinen und Anlagen I & II.* TU WIEN, Institut für Energietechnik und Thermodynamik, 2015.

[13] U.S. Nuclear Regulatory Commission. 2012-2013 information digest. *NUREG-1350*, Volume 24, August 2012.

[14] B. Zarubin. Introduction to light water reactors. *Stanford University*, March 7, 2016.